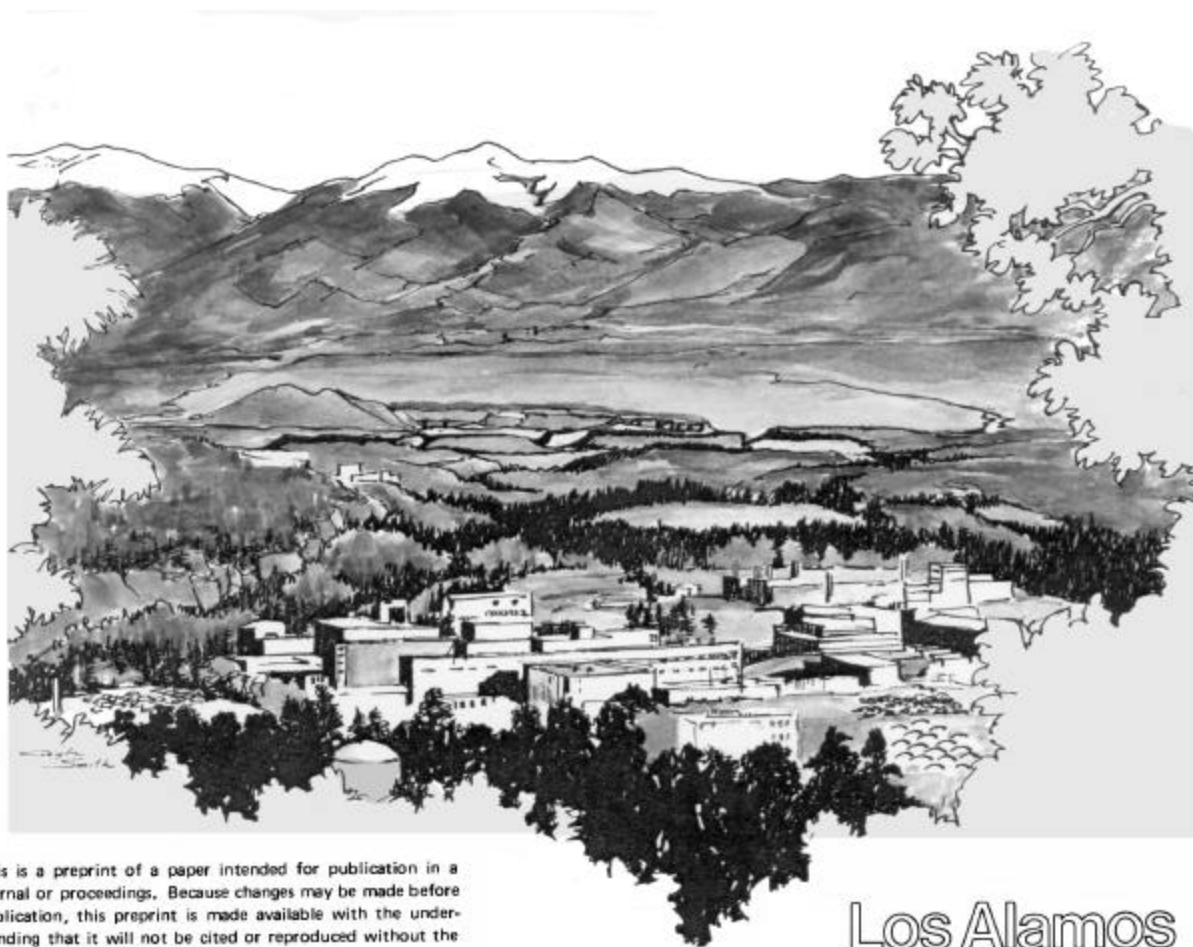


TITLE: Water/Magma Interaction: Physical Considerations
for the Deep Submarine Environment

AUTHORS: Kenneth H. Wohletz, EES-11

SUBMITTED TO: American Geophysical Union Monograph on
Subaqueous Explosive Volcanism



This is a preprint of a paper intended for publication in a journal or proceedings. Because changes may be made before publication, this preprint is made available with the understanding that it will not be cited or reproduced without the permission of the author.

Los Alamos

Los Alamos National Laboratory
Los Alamos, New Mexico 87545

Water/Magma Interaction: Physical Considerations for the Deep Submarine Environment

Kenneth H. Wohletz

*Earth and Environmental Sciences, Los Alamos National Laboratory
Los Alamos, New Mexico, USA*

One might conclude that in deep submarine environments, where hydrostatic pressure is in excess of water's critical pressure, water/magma interaction does not produce expanding vapor and explosive behavior cannot occur. This conclusion is supported by the apparent paucity of hydroclastic material in samples recovered from deep submarine environments. Analog molten fuel-coolant interaction (MFCI) experiments, however, demonstrate explosive dynamics for conditions where water is pressurized above its critical pressure before interaction; MFCI theory further indicates this explosive potential. Thermodynamic predictions show that the conversion of thermal to mechanical energy is only high enough to support explosive behavior for a narrow range of water/magma mass ratios. In submarine environments, apparent mass ratios are too high for explosive behavior, but effective mass ratios (those determined from the water and magma directly involved during interaction) depend upon characteristic times, determined by the sound speed of the water and interface geometry. At high pressure, a supercritical fluid film grows at the water/magma contact surface and can become unstable. With instability the film oscillates, rapidly expanding and collapsing, with a periodicity of milliseconds or less. Each film collapse imparts kinetic energy into the magma, causing magma fragmentation, especially where quench contraction has weakened the magma. With fragmentation more magma surface area is exposed to water, and the film growth/collapse process escalates. When perturbed by some external pressure wave, the unstable film is prone to a detonation-like phenomenon that causes rapid, localized vapor expansion even at high ambient pressure.

1. INTRODUCTION

The earth's oceans cover over 60% of its surface; hence, much of earth's volcanism and volcanic products are hidden from direct view by deep water. Deep seafloor observations by submersible vessels have provided visual and sample documentation of only a miniscule portion of submarine volcanic terrain and likewise seafloor drilling samples represent only an insignificant portion of the volcanic products thought to cover much of the deep ocean basins. Submarine volcanism is significant not only because of volume considerations but also because magma is known to dynamically interact with water. Called *hydrovolcanism* in general, volcanism involving contact of magma with external water occurs in a wide variety of environments and exhibits a range of eruptive phenomena from passive lava quenching to development of extensive hydrothermal systems to enormous explosive eruptions, characterized by

production of steam in vapor explosions. In all cases of hydrovolcanism that have been observed, steam production is a key phenomenon that signifies the interaction.

Submarine hydrovolcanism [Bonatti, 1967] occurs within deep (>200 m) saline water [Honorez and Kirst, 1975] as opposed to shallower (<200 m) *epieiric* and *littoral* hydrovolcanism [Wentworth, 1938; and Mattox and Mangan, 1997]. This type of volcanism is thought to be most common at oceanic spreading centers and on large submarine volcanoes that form flat-topped *guyots* [Cotton, 1969], consisting of pillow basalts and *hyaloclastites*, which are the angular, glassy shards formed by rapid quenching of magma during its interaction with external water in a subaqueous environment.

Whereas shallow submarine to littoral eruptions are known to be capable of explosive behavior (e.g., Myojin Reef in 1952; Capelinhos in 1958; Surtsey in 1963) explosive hydrovolcanic eruptions in the deep submarine envi-

ronment (>2000 m) have not been directly observed but only surmised from observations of deep seafloor hyaloclastites and related phenomena [Haymon *et al.*, 1993; Batiza *et al.*, 1984; Lonsdale and Batiza, 1980; Clague *et al.*, 2000; and Clague, this volume]. Smith and Batiza [1989] found that hyaloclastite deposits occur commonly around summits of seamounts near the East Pacific Rise, showing evidence of hydrovolcanic but not necessarily explosive origins. In some cases these deposits of hyaloclastite resemble deposits of pyroclastic density currents that have spread out from unidentified vents; these have been termed *sheet hyaloclastite*, and their origin is interpreted as disruption of lava flows by water-saturated sediments trapped beneath them [Maicher *et al.*, 2000; and Maicher and White, 2001].

Smith and Batiza [1989] incorrectly concluded (as will be shown later) that water's reduced volume expansion at depths >2300 m prevents steam explosivity; however they did support the idea of explosive mixing of magma and seawater, presumably by cooling-contraction granulation causing high rates of heat exchange.

Haymon *et al.* [1993] made observations of an eruption on the seafloor that included phenomena such as bottom-water murkiness caused by suspended particulates, near-critical temperature and low salinity vent fluids, and venting of white vapor that transformed to gray smoke above the vent. Those authors discussed these observations as possible evidence for explosive activity, but they misinterpreted the lack of cusped shapes among the blocky, angular shards they collected as not diagnostic of *phreatomagmatic* eruption (hydrovolcanism within the zone of saturation), when in fact they are. However, they did mention the shards' similarity to explosive hydrovolcanic ashes, which seems contradictory if not just a terminology problem.

Kokelaar [1986] defined four classes of subaqueous clastic volcanism, including: *magmatic explosivity*, *contact-surface steam explosivity*, *bulk interaction steam explosivity*, and *cooling-contraction granulation*. These definitions are strictly qualitative and thus somewhat ambiguous in physical application, but Kokelaar [1986] provided a guide for the depth limitation of these classes. However, those depth limitations appear to be simplistic and not fully representative of magmatic processes [e.g., Dudás, 1983] or hydrovolcanism (as will be discussed). For example, Kokelaar [1986] limited bulk interaction steam explosivity to depths at which hydrostatic pressure is less than water's critical pressure, based on his interpretations of experiments and observations, but he did not provide hydrodynamic justification for this limit.

Because observed explosive hydrovolcanism is always associated with production of vast quantities of steam and the explosive energy is thought to be derived from the thermodynamic work of steam expansion, an important question arises about the effects of ambient pressure in the

deep submarine environment below a depth of 2200 to 3000 m (depending on salinity), where hydrostatic pressure is greater than the critical pressure of seawater. Over the last 40 years many workers have followed stipulations posed by McBirney [1963] and assumed that supercritical ambient pressure precludes the formation of steam, and thus explosive dynamics are not possible. Because the hydroclastic products (hyaloclastite) that result from magma fragmentation associated with explosive interaction are rarely observed in deep sea cores (although on seamounts they may be common) and pillow lavas are typically observed, one may conclude that high hydrostatic pressure in the deep submarine environment does in fact make explosive interactions unlikely or impossible.

One must also recognize that not all tephra produced by deep submarine eruption are hydroclastic. The magmatic mechanism of tephra production may also be important. Burnham [1981 and 1983] points out that volatile-constituent exsolution that occurs because of crystallization (second boiling) or rapid pressure decrease (e.g., by failure of vent rocks surrounding a submarine conduit) can produce volume increases up to 50% or more even at ambient pressures of 50 MPa (~5 km depth). The thermodynamic work caused by this volume increase has the potential for explosive release, and it may account for extensive magma fragmentation such as the volcanic products associated with Kuroko ore deposits [Tanimura *et al.*, 1983] that formed in deep water (up to 3500 m). Such findings are also emphasized by Dudás [1983].

With a broad overview and discussion of deep submarine pyroclastic eruptions given by Head and Wilson (this volume), this paper focuses on experimental results and theoretical considerations that bear on whether or not hydrovolcanism in the deep submarine environment can produce explosive magma fragmentation. A working definition of explosion is the sudden and rapid production of gas, heat, noise, pressure, and in many cases, a shock wave. Two basic types of explosion are: (1) *detonation*, which is a supersonic propagation of a combustion wave that causes nearly instantaneous vapor release and expansion; and (2) *deflagration*, which is a rapid but subsonic propagation of a combustion wave. For certain circumstances, the word *combustion* can be replaced by *vaporization* in these definitions of explosion.

In the following discussions of explosive submarine hydrovolcanism, I first discuss aspects of the deep submarine environment that play an important role, namely the mode of magma extrusion, the compositional effects of seawater, and water's thermodynamic behavior and variability near the critical point (or critical curve for seawater, see below). Although many molten fuel-coolant interaction (MFCI or FCI) experiments [e.g., Zimanowski *et al.*, 1997a] are not directly linked to the high water abundance and hydrostatic pressure conditions in deep submarine environments, those

discussed in this paper do include these important links. Pertinent MFCI experiments help establish the potential for explosive behavior that can then be considered in light of water/magma interaction physics. The physics are complex and in no way can be completely addressed in this paper, but following on previous studies of hydrovolcanism [e.g., *Sheridan and Wohletz, 1983*] the important parameters of water/magma mass ratio and confining pressure will be specifically addressed. Other theoretical aspects to be considered are the pressure- and temperature-dependent thermal equilibrium between magma and water, the hydrodynamic behavior of supercritical water in response to pressure fluctuations, and the role of *detonation* physics in explosive vaporization.

Overall, the reader should consider this topic an “open book” and realize the limitations of geological observations as well as those of theory and experimentation. In doing so, I hope that the discussions presented help set a basis for future observational and diagnostic studies of submarine hydrovolcanism, stimulate open mindedness to the realm of possibilities, and promote the idea that the problem is not easily constrained.

2. THE DEEP SUBMARINE HYDROVOLCANIC ENVIRONMENT

Two fundamental aspects of the deep submarine hydrovolcanic environment are the magma and the seawater. For the magma its composition and extrusion rate determine how it is introduced to the seawater. For the seawater its phase relationships and thermodynamic properties are important. An additional consideration is the quantities of magma and water that are directly involved during submarine eruption.

2.1. Magma

Because of the mechanics of seafloor spreading and hot-spot volcanism, basaltic compositions are found to dominate the deep submarine environment; however, silicic compositions also exist, especially in arc settings but also along spreading ridges as well [*Stoffers et al., 2002*]. Four generalized modes of magma extrusion are schematically portrayed in Figure 1, but these are by no means comprehensive. Depending upon the flow rate of magma within a conduit below the seafloor, the violence of the eruption, and the magnitude and rapidity of magma and fluid volume changes, seismic disturbances may accompany extrusion. All of these factors are important when considering the dynamics of water/magma interaction.

For mafic (basaltic) magmas, one can consider two end-member extrusion types: (1) slow extrusion rates that tend to form lava flows whose thickness is largely controlled by rheological properties (Fig. 1a); and (2) fast extrusion rates

that tend to produce a fountain-like structure (Fig. 1b). For fast extrusion rates, magma's volume change by crystallization and volatile exsolution may play a role, and the motion of the extruding magma is typically vertical, causing it to rise like a fountain above the seafloor before gravitation forces cause it to settle downward. During its relatively rapid rise from the seafloor, shear stresses on the surface of the magma fountain may exceed surface tension resulting in tearing and separation of magma globules and smaller fragments [cf. *Head and Wilson, this volume*]. The larger globules then may cascade to the seafloor, producing a kind of spatter rampart around the vent, whereas smaller fragments may be entrained in convectively rising seawater that is heated by the magma. These smaller fragments produce a shroud around the fountain, perhaps resembling the fluid issuing from black smokers at spreading-center hydrothermal vents.

Silicic magmas can contain significant portions of dissolved volatiles. During extrusion, magma volume may change significantly by crystallization and volatile exsolution. Crystallization caused by magma cooling and extrusive pressure release promote volatile oversaturation and exsolution. This process has been well described for the submarine environment by *Burnham [1983]*. The mechanical work involved with magma volume changes results in magma fragmentation by both brittle and viscous processes. In this fashion an extruding dome of viscous silicic magma may develop a carapace of hyaloclastite (Fig. 1c). If the volatile oversaturation is high and extrusion dynamics (such as abrupt failure of confining conduit walls) promote a catastrophic decompression of magma, a vent may erupt a column of supercritical fluid and magma fragments (Fig. 1d). As the column rises, the fluid expands and produces momentum that allows further decompression within the conduit, prolonging the eruption.

2.2. Seawater

Seawater is a solution dominated by the presence of salts (mostly NaCl), and its thermodynamic behavior can be approximated by the two-component system of pure water and NaCl. Figure 2a illustrates a P-T phase diagram for the system NaCl-H₂O that shows phase boundaries of the pure components and projections of the phase boundaries for intermediate compositions. The salinity of seawater results in critical behavior not occurring at a single point but along a curve that connects the critical points of the two pure endmembers. These phase relationships show that at any temperature two fluid phases can coexist and a single critical point does not exist if solid NaCl is present. Depending upon local salinity, critical behavior occurs at pressures and temperatures elevated from those of pure water (22 MPa and 647 K) to values approaching ~30 MPa and ~680 K for seawater with a salinity of 3.2 wt % NaCl [*Bischoff*

and Rosenbauer, 1988], and critical pressure is expected at a depth of ~3 km in the submarine environment. Also, Figure 2a shows that as seawater is heated, solid NaCl is precipitated, which may greatly affect vapor nucleation [cf. White, 1996].

The two-phase boundary of seawater [Bischoff and Rosenbauer, 1984] is similar to that of pure water for subcritical conditions in pressure-temperature space (Fig. 2b), but unlike pure water, it does not end at the critical point, but projects nearly linearly to higher pressures and temperatures (~680 K at 30 MPa to ~750 K at 50 MPa). Below the critical point the two-phase region of seawater consists of liquid and low-salinity vapor, and above the critical point it consists of brine and high-salinity vapor. These phase relationships indicate that a vapor phase can exist in seawater at supercritical pressures.

Another effect of the dissolved solids in seawater is a decreased heat capacity compared to that of pure water. This effect can be approximated [Buntebarth and Schopper, 1998] as:

$$C_{sw} = x_w C_w + (1 - x_w) C_s, \quad (1)$$

where C_w and C_s denote the constant volume heat capacities of pure water and dissolved constituents respectively and x_w is the pure water mass fraction. Dissolved solids in seawater range from about 0.7 to 4.5% by mass with the standard average being 3.5% [Turekian, 1968]. Using Eq. (1) the heat capacity of seawater (C_{sw}) is several percent lower than that of pure water; however, as discussed below, since the heat capacity of pure water varies by approximately a factor of 2 over most of the range of pressure and temperatures typical of hydrovolcanism, the bulk heat-capacity effect of dissolved solids in seawater is relatively small. The following discussions assume that heat capacity and phase transition effects of seawater have offsetting effects for situations of rapid heating such that pure water provides a workable proxy.

Because water/magma interaction can result in a relatively high-pressure and high-temperature water phase, it is important to consider the variability of water near critical point (curve) conditions. Figure 3 illustrates the variation of heat capacity, viscosity, and expansion coefficients at 30 and 60 MPa, analogous to deep submarine environments at about 3000 and 6000 m depth, respectively. Note that heat capacity, viscosity, and the isobaric expansion coefficient vary rapidly in the range 600-800 K, near water's critical-point temperature (647 K). This means that small changes in temperature produce large changes in properties that determine how water behaves thermodynamically and hydrodynamically. If large thermal gradients exist near the contact of water with magma, which is to be expected in hydrovolcanism, then high pressure and velocity gradients

will also exist, and perturbations in water movement result in the likelihood of hydrodynamic instability. For example, a supercritical fluid subjected to small pressure perturbations may tend to oscillate [Greer and Moldover, 1981] in density between liquid and vapor states (e.g., growth and collapse of vapor bubbles). The speed at which water flows from higher to lower pressure regimes depends not only on the magnitude of the pressure gradient but also on its viscosity; rapid viscosity fluctuation may enhance or dampen convective currents. It is a chaotic *thermal-hydraulic* system that has received considerable attention for over two decades from nuclear engineers concerned with coolant flow stability in nuclear reactors [e.g., Ruggles *et al.*, 1989 and 1997].

2.3. Water/Magma Interaction

Interaction of water with magma involves heat transfer from the magma to the water and chemical species migration driven by solution and precipitation. In submarine environments, the mass of water present typically exceeds that of magma by orders of magnitude, such that heat transfer produces only localized water temperature and compositional gradients that rapidly dissipate. However, the amount of water that dynamically interacts with the magma can be quite variable. Where water becomes entrapped by magma either within the vent conduit, beneath lava flows (as wet sediment), or by engulfment during rapid extrusion, the mass of magma may exceed that of water during interaction. On the other hand, at lava flow top surfaces, convective currents might involve a much larger mass of water than that of magma, promoting passive interaction. The chemical dynamics of water/magma interaction are very important to the evolution of seawater and hydroclast compositions; however the physical dynamics are the focus of this paper.

3. MOLTEN FUEL-COOLANT INTERACTION EXPERIMENTS

Peckover *et al.* [1973] gave the first published accounts of molten fuel-coolant interaction in submarine volcanic explosions. Their work closely followed Colgate and Sigurgeirsson's [1973] study of the MFCI explosive hazard of lava-flow diversion by quenching it with water. In 1976 after discussions with Stirling Colgate, I began MFCI experiments as analogs for water/magma interaction [e.g., Wohletz, 1980; Wohletz and McQueen, 1984; and Wohletz *et al.* 1995], drawing on the expertise rapidly developing in the fields of nuclear and mechanical engineering in application to nuclear reactor safety [e.g., Buxton and Benedict, 1979]. Bernd Zimanowski and his colleagues began similar experimentation in the mid 1980s, and they continue a very fruitful MFCI experimental program to the present time

[e.g., Zimanowski *et al.*, 1986, 1991, and 1997a]. These experiments demonstrate a wide range of dynamic phenomena caused by the interaction of a melt (fuel) with water (coolant). Experimentation has also shown that confining pressure likely plays an important role in controlling the nature of the phenomena. One must consider the limitations of such experiments in reproducing the submarine environment, and such limitation concern the experimental design (geometry) and method by which the melt is introduced to the water. In this light, the MFCI experiments conducted by Wohletz *et al.* [1995] and Zimanowski *et al.* [1991 and 1997a] have notable differences, and thus experimental results have distinct contrasts, but general similarities persist nonetheless. For the following discussions, I focus on the Wohletz *et al.* [1995] results, noting that Zimanowski [this volume] has different conclusions, based on his experimental results.

Previous papers [Wohletz *et al.*, 1995; and Wohletz, 2002] have addressed the adequacy of using a thermite melt as a basalt analog and for study for the initial seconds of water/melt interaction. Melt temperature, density, viscosity, enthalpy, and surface tension are important factors, and the thermite analog is similar to basalt except its enthalpy is about 3 times that of basalt. A second consideration for application of these experimental analogs is the manner by which high pressure is attained prior to water/melt interaction; the experiments are self-pressurized, which will be discussed later. Finally, experimental results have shown that the bulk water/melt mass ratio appears to be a primary factor controlling the dynamics of the interaction. For submarine volcanism, this ratio is apparently very high, but the actual amounts of water and magma contributing to an interaction may be strongly dependent upon the control volume considered. The following experimental results for high water/melt ratios (assumed to be analogous to submarine conditions) have important bearing on understanding factors that control interactions in an environment where the volume of water is much greater than that of magma.

The *water-box* experiments [Wohletz *et al.*, 1995] utilized Plexiglas box of ~1-m width, length, and height (Plate 1). Thermite was placed within the box in a steel canister stack, ~0.3 m in diameter, ~1 m in height, and containing ~100 kg of thermite. The box was then filled with about 900 kg of water, giving a high water/melt ratio. After the thermite was ignited and became fully molten, it eventually melted through the canisters and contacted the water. The ensuing water/melt interactions lasted a number of minutes, dominated by flow of molten globs of melt at the base of the box and ballistic, Strombolian-like activity near the top of the box (Plate 2). These experiments varied in their violence with time, and one that displayed mild Strombolian play for several minutes ended abruptly in a violent Surtseyan-like blast. Investigation of the products from these

experiments showed that less than half of the thermite melt formed pillow-lava-like globs that remained within the box and the rest was fragmented to scoriaceous, centimeter-sized fragments mostly ejected out of the box. These experiments not only demonstrate the quenching ability of water at high interaction ratios but also the variability of interaction violence, depending on the location of the interaction at the base of the box (passive) or at the surface of the water (mildly explosive). However, these experiments did not address the effects of hydrostatic pressure, which will be covered in the following results for high pressure experiments.

In review of experiments [Wohletz *et al.*, 1995] that best simulate high hydrostatic (confining) pressure, strong evidence is given for the potential of supercritical explosion in MFCI phenomena. Those experiments involved the use of a confinement vessel (Plate 3) that allowed development of supercritical pressure prior to burst. Pressure vessels of several sizes were used, and they contained from 3 to 90 kg of molten thermite in which quartzo-feldspathic sand was mixed to more closely simulate basaltic compositions. Water (typically one-quarter to one-third the mass of thermite) filled the base of the vessels, separated from the thermite above by an aluminum plate. The melting process initiated at the top of the vessel and proceeded downward until the molten thermite perforated an aluminum plate and then directly contacted water. This design simulated the rise and injection of magma onto the seafloor by utilizing gravitational force of the melt. Although this design is inverted compared to natural systems, a vent pipe was used in some experiment designs; it extended from the vessel top into the water compartment and insured that the release of water pressure was not impeded by the melt. A burst valve at the bottom of the vent pipe allowed pressure to rise to a specified level prior to onset of vapor expansion.

Plate 4 shows a supersonic jet of melt fragments and superheated steam rising >30 m above the experimental vessel and a plume of micrometer-sized dust (quenched melt fragments) convectively rising above the jet. This example illustrates the typical burst phenomena for high-pressure experiments. Example pressure records from high-pressure experiments are displayed in Figure 4. In order to interpret these pressure records, several aspects of this experimental design must be mentioned, and these considerations clarify the analogy to submarine hydrovolcanism. The zero-time for the pressure records is arbitrary, since the time required for the thermite to become fully molten and contact the water varied among the experiments. Important to this experimental design is that pore-gas expansion during thermite melting contributed much of the vessel pressurization prior to the contact of the melt with water; it also led to premature vent failure in some experiments for which the ejected debris showed lumps and clots typical of incomplete interaction. The time of

burst (vapor explosion) is marked by the rapid pressure decline, as confirmed by dnematography. Typically, the thermite gradually pressurized the system in ~ 1 s prior to contacting the water, after which the pressure rose precipitously in a few milliseconds before bursting.

Difficulties in monitoring pressure in these experiments include gauge damage by the violence of the interaction (Fig. 4a) and gauges recording different pressure histories at different positions within the vessel (Fig. 4b). Figure 4a shows results for an experiment where one pressure gauge showed little or no response (damage confirmed by post-experiment examination) while another gauge recorded a pressure of approximately 35 MPa prior to burst. Figure 4b shows an initial burst (dashed curve) occurred at the designed bursting pressure (6.8 MPa) and a secondary burst occurred ~ 0.5 s later at ~ 9 MPa. This double-burst was recorded by another transducer as a single event that reached a pressure of 23 MPa, demonstrating that interaction pressure is not the same for all locations in this dynamic system, possibly a manifestation of multiphase effects and multiple shock-wave domains. Figure 4c shows the interaction pressure rapidly rising to >50 MPa approximately 0.5 s before the major burst. A small pressure spike ~ 0.1 s before the main pressurization likely reflects an initial vapor-film growth and collapse event before wholesale interaction occurred, while the third pressure spike was an event caused by residual water and melt in the vessel after the main burst. Figure 4d records burst at 23 MPa just above critical pressure. Figure 4e shows bursting from pressure exceeding 60 MPa, whereas Figure 4f records bursting at a pressure just below critical. It is important to note that the time scale for these pressure plots is too large to show detail of the pressure history caused by water/magma interaction just prior to burst. Our interpretations of many pressure records is that once full water/melt interaction begins, pressure builds to its maximum within a few milliseconds or less before burst. This means that for these experiments full interaction and bursting are nearly simultaneous events and most of the interaction occurred near the peaks of the pressure curves shown in Figure 4.

General results indicate that experiments designed to pressurize above critical pressure did in fact show explosive interaction. A smaller fraction of the high-pressure experiments attained explosive interaction than did low-pressure ones; however, those high-pressure experiments that exploded, did so with markedly increased energy [Wohletz *et al.*, 1995]. These experiments also showed maximum pressure well in excess of burst pressure, indicating pressure grew faster than it could be relieved, a shock-wave phenomena. Two other general results are noted but not well understood. When designed confining pressure was >35 MPa, experiments showed exponential increases to supercritical pressures in less than a second prior to vapor explosion (commencement of rapid expan-

sion), whereas those confined at pressures near critical showed slower rises and lower maximum pressures. Overall these experiments demonstrate that not only can water/melt interaction produce supercritical burst pressures, they can also occur where confining pressure is supercritical prior to burst.

4. THERMODYNAMICS AND WATER/MAGMA MASS RATIOS

The water/melt mass ratio, R , was experimentally identified by Wohletz and McQueen [1984] as an important control of interaction dynamics, determining the violence of the interaction and whether it is explosive or not. Although R is difficult to quantify in nature [cf. White, 1996], thermodynamic predictions at atmospheric pressure and numerous semi-quantitative and qualitative observations for near-surface environments support this theory [e.g., Wohletz, 1986]. In order to apply this theory to the deep submarine environment, one can adapt thermodynamic calculations for high ambient pressures.

Where careful and detailed observations constrain magma and water flux, such as in a terrestrial setting of a known aquifer and a witnessed eruption [e.g., Ort *et al.*, 2000], inferred values of R for various phreatomagmatic eruption types fit quite closely with thermodynamic predictions. The abundance of pillow lava in submarine settings also qualitatively supports experimental results. However, where water is abundant, it is difficult to establish constraints on just how much of it actually interacts with erupting magma. Thus for the submarine environment, only *apparent* mass ratios (those ratios unconstrained by a defined control volume) can be determined ($R \gg 10$). From the aforementioned experimental evidence and by the theory to be presented, such mass ratios are much too high to explain explosive interactions in the submarine environment. As discussed earlier, the actual involvement of seawater with magma may be influenced by partial or full enclosure of a volume of water by magma, in which cases the *effective* mass ratio (a mass ratio that measures the actual amounts of water and magma involved in heat exchange) may be <1 .

4.1. Hydrostatic Pressure Effect

The approach to calculating the thermodynamic work produced by water/magma interaction involves three primary assumptions, based on the Hick-Menzies [1965] approach as discussed by Wohletz [1986] and Wohletz *et al.* [1995]. These assumptions are: (1) during interaction water can be treated as a single-component (pure) substance; (2) water and magma reach an initial equilibrium temperature at nearly constant volume prior to expansion; and (3) the expansion phase can be approximated by two thermodynamic

cases. These thermodynamic cases are: (1) *isentropic fluid* in which the water expands at constant entropy as an idealized “frictionless” adiabatic process; and (2) *isentropic mixture* in which the water expands while being continuously heated by magma fragments enclosed by the water. For brevity I will refer to these two cases as *fluid* and *mixture*, respectively. Whereas Kieffer and Delany [1979] critically assess *isentropic fluid* decompression within a geological context, there is little precedence for evaluation of *isentropic mixture* decompression in this context. Self *et al.* [1979] suggested using the term *isothermal* for the nearly constant-temperature expansion of vapor in contact with tiny magma fragments. This terminology, which Wohletz [1986] and Wohletz *et al.* [1995] attempted to fit to MFCL, implies the assumption that the mass of fragments greatly exceeds that of the vapor and heat transfer over the large surface area of the fragments is fast enough to keep the vapor at nearly a constant temperature during expansion. For water/magma interaction where R and fragment size can vary over an order of magnitude, the *isothermal* terminology does not strictly apply.

The initial equilibrium and expansion assumptions are idealizations that allow one to constrain the maximum pressure, temperature, and volume that water attains during interaction. Certainly many factors limit the validity of these assumptions, and these factors include most notably the time scales on which heat transfer and phase separation occur. If water expands and separates from the magma heat source prior to reaching initial thermal equilibrium with the magma, then the interaction thermodynamic work will be minimized. Although this possibility is best modeled by the *fluid* expansion case, that model still assumes an initial thermal equilibrium. On the other hand, the *mixture* expansion case assumes no separation of water from the magma during expansion, and thus, it is difficult to constrain for a situation where the initial thermal equilibrium does not occur.

Heat transfer between the magma and water is dominated by conduction and convection; the thermal absorption coefficient of water is too low for effective radiative heat transfer within a control volume, except in certain cases of film boiling [Dinh *et al.*, 1998]. Experiments show that water/melt interaction can involve a commingling phenomenon that occurs prior to thermodynamic expansion and flow. This commingling involves the rapid breakdown of the melt into a mixture of fine particles with water that has been called an *explosive premixture*. The melt fragmentation in this premixture produces the high surface areas needed for heat transfer rates fast enough for thermal equilibrium to occur before expansion. The premixture also promotes thermodynamic expansion of the water in intimate contact with fine melt particles, as modeled by the *mixture* case, which predicts an upper limit for thermodynamic work production. If during expansion the water

separates from the melt particles, then the *fluid* case applies and provides a measure of the lower limit for thermodynamic work production. As shown later, for deep submarine conditions where ambient pressure is high, *mixture* expansion may be a necessary condition for explosive behavior.

Based on the assumptions above, some thermodynamic predictions (Appendix A) highlight the potential effects of water/magma mass ratio and hydrostatic pressure on interaction dynamics. Figure 5 shows details about calculated, pre-expansion, equilibrium conditions and the thermodynamic paths for expansion for the *fluid* and *mixture* cases. For the following examples, water is at 277 K (near its densest state) and the magma is basaltic (~1500 K) because it is volumetrically dominant in the deep submarine environment. Similar results are expected for much less common silicic magmas. With slightly different heat contents but lower extrusion temperatures than basalt, silicic magma heat contents are about 75% of that of the basalt considered here, a consideration [Wohletz, 2002] that will have a corresponding effect on results presented here.

Figure 5a shows that calculated initial equilibrium states are a strong function of R and exceed critical pressure for R values <2.0 . The initial equilibrium states also show specific volume increasing with decreasing R ; but that increase amounts to a $<2\%$ increase in the mixture volume at $R = 0.01$. Although increasing ambient pressure decreases the equilibrium entropy, this effect is too small to portray in Figure 5a. Water expansion follows isentropes (Fig. 5a) to a pressure of 0.1 MPa (atmospheric pressure); for expansion to higher ambient pressures typical of deep submarine conditions, the final expansion state in Figure 5a is simply the intersection of an isentrope with a horizontal line (isobar) at the ambient pressure. Clearly greater expansion is achieved for interactions at lower R values, which by Appendix A, indicates greater thermodynamic work per unit water mass. For most R values, expansion to 0.1 MPa ends in the steam dome (two-phase region of liquid plus vapor). For cases of expansion to 10 MPa, if $R > 1$ then there is little or no vapor production and thermodynamic work; in contrast, if $R < 0.1$ then expansion produces superheated vapor and high amounts of thermodynamic work per unit mass water. For cases where the ambient pressure is supercritical, if $R > 0.5$ then isentropes are so steep that little volume change occurs along them and the resulting thermodynamic work is small. However, with increasing supercritical ambient pressure, the initial equilibrium pressure increases so that the thermodynamic work also increases.

Figure 5b illustrates the *mixture* case for which water entropy increases during expansion because the water is continuously heated by hydroclasts entrained in it. The entropy increase with expansion is shown by straight lines in Figure 5b for simplicity, but these lines may be slightly

curved because the temperature and pressure dependence of conductivities, especially in the steam dome where conduction to liquid and vapor components does not occur at the same rate. Because *mixture* expansion takes water to higher entropies, it produces more thermodynamic work than does expansion in the *fluid* case. The dashed lines in Figure 5b show the small but finite effect of hydrostatic pressure on the initial equilibrium at various R values. With increasing ambient pressure, the initial equilibrium entropy decreases. For the expanded states, example isobars drawn at 0.1 and 10 MPa show that increasing hydrostatic pressure limits expansion to decreasing final entropy (lower volume) states. Accordingly, the pressure-volume work is limited by hydrostatic pressure. However, as will be discussed later, it is not correct to assume that expansion stops when ambient pressure is reached for dynamic interactions where shock waves are formed and sound speeds vary considerably over short distances.

What do these thermodynamic calculations show other than the fact that they predict a hypothetical initial equilibrium states that are above the critical pressure for all R values <2 and above 100 MPa (~ 10 km depth) for R values <0.6 ? First of all one should note that in the supercritical region, isentropes become steeper with increasing pressure such that pressure change produces less and less volume change, especially for R values >0.5 . This observation suggests that as supercritical ambient pressure increases, *fluid* expansion produces less and less thermodynamic work. In contrast, the *mixture* case shows that for expansion at R values <0.4 , water entropy increases (while the mixture is entropic) from $4 \text{ kJ kg}^{-1} \text{ K}^{-1}$ to values that reflect higher volumes; thus, in the supercritical region, the *mixture* case produces more thermodynamic work than does the *fluid* case.

To evaluate the thermodynamic work potential for interactions at different R values, Figure 6 shows plots of thermodynamic conversion ratios, which represent the percentage of the magma's thermal energy converted to thermodynamic work, approximately half of which might be manifested as melt-fragment kinetic energy [Wohletz *et al.*, 1995]. For the cases of *fluid* and *mixture* expansion, two endmember final states are shown, one for expansion to hydrostatic (ambient) pressure and one for expansion to 0.1 MPa. Whereas expansion to hydrostatic pressure is intuitive, the other endmember represents full expansion to atmospheric pressure, which is approachable under certain conditions of shock-wave propagation and other factors to be discussed. First of all, the *mixture* cases produce higher conversion ratios than do the *fluid* cases as also do full expansions to 0.1 MPa compared with those limited to expansion to hydrostatic pressure. For the *fluid* hydrostatic endmember (Fig. 6a), the effects of ambient pressure are not intuitive (because of the effect of R on the initial equilibrium state). Below the critical pressure, conversion ra-

tios decrease with increasing ambient pressure (i.e., 0.1, 10, and 20 MPa), but above the critical pressure conversion ratios rise with increasing ambient pressure (i.e., 40, 60, and 80 MPa). The trend for the *mixture* hydrostatic endmember (Fig. 6c) shows decreasing conversion ratios with increasing ambient pressure. In contrast for the 0.1-MPa endmembers (Fig. 6b and 6d), both the *fluid* and *mixture* cases show increasing conversion ratios with increasing ambient pressure.

In order to further describe these conversion ratio calculations, a horizontal line is drawn in Figure 6 at a conversion ratio of 2.5%, designating an explosive threshold. This value represents the minimum conversion ratios calculated for experiments [Wohletz *et al.*, 1995] that produced demonstrably explosive behavior and complete melt fragmentation. In deference to the limitations of drawing analogies from these experimental results, this explosive threshold is considered to be arbitrary. The result of this consideration is that water/magma interactions are capable of being explosive up to hydrostatic pressures of 80 MPa, which represents a depth of 8000 m. Higher hydrostatic pressures, which have not been calculated, are also expected to be capable of explosive work production with the notable exception of the *mixture* hydrostatic endmember (Fig. 6c), which shows conversion ratios declining below the explosive threshold as ambient pressure exceeds 80 MPa. Another aspect of the results shown in Figure 6 is the range of R values over which explosive behavior might be attained for subsurface interactions (hydrostatic pressure >0.1 MPa). This range extends from $R \approx 0.1$ -1.3 (hydrostatic endmembers) and from $R \approx 0.1$ -3.0 (0.1-MPa endmembers). Whereas increasing pressure always increases this range for both 0.1-MPa endmembers, it decreases the range to $R \approx 0.1$ -0.7 for hydrostatic endmembers at ambient pressures found at depths from 1000 to 4000 m. The range of explosive R values for the mixture hydrostatic endmember strongly decreases with increasing pressure, becoming negligible at pressures above 80 MPa.

In summary of hydrostatic pressure considerations, both 0.1-MPa endmembers show the greatest likelihood (with respect to R values and pressure) for conditions necessary for deep submarine explosive interactions. For the hydrostatic endmembers, increasing pressure generally decreases the likelihood of explosive interaction. Overall, predicted explosive interaction requires R values that seem very small, considering the abundance of water in submarine environments; thus, the question arises as to whether such conditions are really applicable, which is the subject of the next section.

4.2. Effective Water/Magma Mass Ratios

Effective mass ratios depend upon characteristic times and lengths, determined by the propagation speed of ther-

mal and pressure waves and by the interface geometry. Such parameters control just how much water actually is involved in the interaction heat exchange. For magma, conductive heat transfer times and lengths are important. For seawater, conductive and convective transport dominate, and radiative transport plays a role only where supercritical water loses its transparency *Dinh et al.* [1998]. On the other hand, a multitude of geometric possibilities can be imagined from a simple planar interface to entrapment and engulfing configurations to rapid mixing of water and magma fragments in a erupting lava fountain [e.g., *Batiza et al.*, 1984; *Smith and Batiza*, 1989; *Head and Wilson*, this volume; and *Clague*, this volume]. For each possibility the linear dimensions determined by characteristic lengths and times can be constrained. The example given in Figure 7 is just one possible configuration that serves as an example how an effective mass ratio might be evaluated.

Figure 7 depicts an hypothetical contact of seawater over a rugose lava flow surface, such as might be caused by rapid extrusion rates or development of pressure ridges [cf. *Maicher et al.*, 2000]. For this case one can simply estimate the effective interaction ratio by volume ratios, defined by characteristic lengths. In order to define characteristic lengths (L ; subscripts w and m denote water and lava respectively), a characteristic time, t_c , must be defined that takes into account both the thermal and fluid dynamics involved. From the experiments discussed earlier, this characteristic time is linked to the periodicity of water pressurization and expansion.

Consider the growth of a supercritical-fluid film at the contact interface shown in Figure 7. Expansion of this film continues while its pressure is greater than the surrounding seawater. It also creates a pressure wave that propagates into the seawater at the speed of sound and eventually reflects off an impedance (the product of density and sound speed) discontinuity, which for this example is a spine of lava at a distance, L , from the film surface. Such an impedance boundary might also be the substrate for a situation where water is trapped below a lava flow or the other side of a cavity in which water is surrounded by lava. When the reflected wave strikes the surface of the film, the film is partially or fully destabilized, setting a characteristic time:

$$t_c = 2L/c \quad , \quad (2)$$

where c is the sound speed of water ($\sim 1500 \text{ m s}^{-1}$ for seawater). This reasoning is very simplistic: a multitude of pressure perturbations likely exist with a spectrum of travel times for which some period or range of periods is dominant. For this argument, let Eq. (2) define an average characteristic time. The characteristic length for seawater, L_w , is a measure of how far a thermal wave moves into the water in the characteristic time; it can be simply stated as:

$$L_w = v_c t_c \quad , \quad (3)$$

where v_c is growth speed of the supercritical fluid layer. *Dinh et al.* [1998] quantify *film boiling* heat transfer for FCI conditions and report vapor film speeds that increase with water temperature. For fully developed film boiling at temperatures $< 1000 \text{ K}$, these speeds are $< 5 \text{ m s}^{-1}$, and because film boiling takes time to develop fully, film speeds are likely to be well below 1 m s^{-1} in the first few milliseconds of film boiling [*Corradini*, 1981].

Because the heat flux in the seawater is limited by the heat conducted from the lava, the amount of heat transferred from the lava depends on the characteristic depth (length), L_m , of a thermal wave penetration into the lava over the period of time, t_c :

$$L_m \approx \sqrt{t_c k} \quad , \quad (4)$$

where k is the thermal diffusivity of the lava. From this greatly simplified estimation of L_w and L_m and values for the densities of seawater (\mathbf{r}_w) and lava (\mathbf{r}_m), the *effective* water/magma mass ratio R is:

$$R = (L_w^3 / L_m^3) (\mathbf{r}_w / \mathbf{r}_m) \quad . \quad (5)$$

Although the above estimation of R is quite hypothetical, the following example shows how it might be evaluated. Consider a submarine basaltic lava flow with a rugose surface [cf. *Maicher et al.*, 2000]. For a characteristic dimension L of 1.5 m (Fig. 7) t_c would be $\sim 2 \text{ ms}$. Using typical k values for basalt ($\sim 1 \times 10^{-6} \text{ m}^2 \text{ s}^{-1}$), $L_m \approx 45 \text{ } \mu\text{m}$ from Eq. (4). Because the thermal diffusivity of water at pressures above 22 MPa averages about one-half that of basaltic lava, L_w should be $\sim 0.7 L_m$ for a conduction-dominated system. However, Eq. (3) also takes into account convective and radiative heat transfer; thus, L_w ranges from a conductive minimum of $\sim 20 \text{ } \mu\text{m}$ to an incipient film boiling value of $\sim 200 \text{ } \mu\text{m}$. In order to evaluate Eq. (5) densities must be factored in. Basaltic lava density depends upon its vesicularity, and here I will use a value of 2500 kg/m^3 . The density of the supercritical fluid at a temperature of $\sim 1000 \text{ K}$ and pressure of 22 to 50 MPa is between 50 and 110 kg/m^3 . From these values Eq. (5) predicts and *effective* R in the range of 0.01 to 3.8; the lower extent of this range is compatible with R values thought to be typical of terrestrial explosive hydrovolcanism.

Certainly, a more rigorous approach to estimating effective values of R can be developed, and the one shown above is only to illustrate some of the parametric constraints that might be considered. But if characteristic lengths and times are truly important in determining an *effective* R , then one might conclude that explosive erup-

tions are indeed possible in submarine situations, especially for cases where smaller characteristic lengths and shorter times are involved, such as might be associated with high extrusive rates. On the other hand, as characteristic lengths and times increase, film boiling has more time to mature such that L_w increases more rapidly than does L_m , leading to much higher *effective* R values.

With thermodynamic and geometrical considerations that suggest an explosive potential for deep submarine water/magma interactions, the details of how heat transfer from the magma to water can proceed at a rate required to produce dynamic effects needs attention. The dynamics at the water/magma interface involve not only heat transfer phenomena but also hydrodynamic phenomena, those kinetics that describe how water and magma behave in the presence of high thermal and pressure gradients. The following discussion covers considerations that demonstrate that contact interface dynamics might in fact be relatively insensitive to water/magma mass ratios, making the preceding discussions of secondary importance.

5. CONTACT INTERFACE DYNAMICS

Kokelaar [1986] identified two classes of steam explosivity in subaqueous basaltic volcanism: *contact-surface* and *bulk interaction*. The former class concerns the dynamics along an interface between a free body of water and magma, and the latter case applies to the dynamics of a volume of magma that confines water or water-rich clastic materials either within the magma or at its margins. In either case the dynamics begin with an initial contact of magma with water. During this initial exposure, a very thin film of water is nearly instantaneously heated. From considerations of characteristic heat diffusion times for the water and magma, an estimate of this instantaneous contact temperature, T_i , can be made:

$$T_i = \frac{T_m [\mathbf{k}/\sqrt{\mathbf{a}}]_m + T_w [\mathbf{k}/\sqrt{\mathbf{a}}]_w}{[\mathbf{k}/\sqrt{\mathbf{a}}]_m + [\mathbf{k}/\sqrt{\mathbf{a}}]_w}, \quad (6)$$

in which subscripts denote properties of the magma (m) and water (w), \mathbf{k} is the thermal conductivity, \mathbf{a} is the thermal diffusivity ($\mathbf{a}^2 = \mathbf{k}/rC$; C = specific heat capacity; r = density), and T is the initial temperature. For submarine conditions, the values for water are: $T_w \approx 277$ K, $C \approx 4.2$ kJ kg⁻¹ K⁻¹, and $\mathbf{k} \approx 0.6$ W m⁻¹ K⁻¹ with C falling and \mathbf{k} increasing about 1% for every 10 MPa increase in pressure. Magma composition generally dictates T_m with basalts erupting at 1473 to 1523 K; more silicic compositions range from 900 to 1200 K. For magma the specific heat capacity is typically 1.0 to 1.2 kJ/kg-K, and \mathbf{k} ranges from 1.1 to 4.8 W/m-K. These values set T_i in the range of 800-

1000 K, which for neatly constant-volume equilibrium requires an instantaneous supercritical pressure.

5.1. Film Instability

Instantaneous heating of a film of water produces a small shock wave, which moves away from the contact at or above the speed of sound. The film expands in its wake and eventually develops into a region of film boiling, which is not necessarily a stable state. Stability of this vapor film requires that the rate heat is supplied to the film from the magma equals that transferred to the surrounding water. Instability arises where the film expands so fast that it exceeds the volume where it is in thermodynamic equilibrium. It then abruptly condenses, collapsing back on itself. The collapse of the film causes it to impact the magma surface and produce a finite strain in the magma. For certain contact surface geometries, the film collapse can be axisymmetric and produces tiny jets of water that penetrate the magma surface. After collapse, the film is recreated, repeatedly growing and collapsing in a cyclic fashion at a characteristic frequency of several kilohertz or more. The vapor-film oscillation gradually heats the water in the vicinity of the magma surface and causes strain to accumulate in the magma by repeated film impacts and jetting as well as by the volumetric changes caused by rapid magma cooling (quench contraction); the accumulated strain generally produces magma fragmentation. In contrast to this scenario of film instability leading to magma fragmentation, growth of a stable film interface effectively insulates the magma such that fragmentation and quench granulation do not develop, perhaps a reason why pillow lava stay in tact.

Figure 8 illustrates heat transfer associated with film growth and collapse in an idealized spherical system. The conductive factor is the differential change in heat transfer rate with the film thickness (radius) for a constant thermal differential [Wohletz, 1983]. As vapor forms and expands around the melt sphere, it cools, its pressure decreases, and the area over which it conducts heat to the surrounding liquid increases, leading to a decreasing conductive factor. The momentum of the film growth may cause its over-expansion to a thickness where the heat supplied is less than the heat lost and the film pressure is less than ambient. In this case growth is halted when the film spontaneously condenses and collapses. Because of viscous effects, this expansion and collapse cycle is irreversible. During collapse the conductive factor increases at a slower rate than it decreases during expansion, and heat is converted to kinetic energy by an amount that is proportional to the hysteresis of the system. In contrast, a stable film might oscillate around values of unity for conductive factor and film thickness, but it would not grow out of equilibrium nor collapse completely. Stable films might exist where con-

vective heat transport around the film balances conduction from the magma, a situation where passive melt quenching occurs such as in the case of pillow lava formation.

One fate of such contact interface dynamics is production of a coarse mixture of magma fragments, liquid, and vapor. With increasing magma surface area for conductivity, heat transport grows exponentially as an escalating system. Convective currents that develop in response to these dynamics tend to dampen the system so that catastrophic mixing of fragmented magma and water does not occur. If, on the other hand, catastrophic mixing does occur, then the system is not only thermodynamically unstable (because of the film expansion and collapse process), it is also hydrodynamically unstable because of large pressure, density, sound speed, and conductivity gradients produced by the film. Such instability is prone to a kind of detonation, termed *thermal detonation*, especially if perturbed by some external pressure wave, such as that produced by volcanic seismicity.

5.2. Thermal Detonation

The term *thermal detonation* originated during early studies of fuel-coolant interactions for nuclear reactor safety analysis [Board *et al.*, 1975; Bankoff and Jo, 1976; Fauske, 1977; Sharon and Bankoff, 1981; and Yuen and Theofanous, 1995]. Stimulated by the proposal of Fowles [1979] that vapor explosions constituted a kind of elementary detonation, a very radical idea, considering that detonation is classically tied to chemical reactions, Rabie *et al.* [1979] did a rigorous study of rapid phase-change dynamics and concluded that certain materials could display the phenomenon of *polymorphic detonation*. Harlow and Ruppel [1981] used numerical multiphase simulations to demonstrate the plausibility of explosion wave propagation along the contact of two liquids, one above the boiling-point temperature of the other.

The concept of thermal detonation as originally conceived has many shortcomings when applied to real situations of MFCI, several of which are: (1) it requires an unrealistically high trigger pressure; (2) it involves hydrodynamic fragmentation that may not be fast enough to support detonation; (3) it is based on the classical, single-phase, Chapman-Jouguet detonation theory that is difficult to prove for heterogeneous mixtures; and (4) the pressure-wave attenuation caused by the mixture tends to prevent sustained shock-wave propagation. Because detonation is such a specific concept many have argued that it just does not apply to MFCIs, especially from standpoints of required fragmentation rates and premixture ratios [Condiff, 1982; Fletcher and Theofanous, 1995; and Yuen and Theofanous, 1999].

Yuen and Theofanous [1999] show calculations that illustrate why the now classical theory of multiphase thermal

detonation of Board *et al.* [1975] is not physically possible. Their calculations focus on fuel-coolant premixture ratios (volumetric ratio of fuel to water-plus-vapor). For lean ratios, detonation is only possible where the void (vapor) fraction is nearly zero (i.e., $R > 1.5$), a situation where thermodynamic conversions ratios are very low and necessary film boiling is unrealistically precluded. For rich ratios with the physically required film boiling (i.e., $R < 0.05$) only weak detonation is possible. Only for a rather limited range of intermediate premixture ratios (the case examined by Board *et al.* [1975]) for which the volume fractions of fuel, water, and vapor are equal (i.e., $R \approx 0.5$), did Yuen and Theofanous [1999] calculate a stable detonation with a pressure of ~ 150 MPa. However, experimental [Angelini *et al.*, 1992; 1995] and analytical studies [Fletcher and Thyagaraja, 1991] show that such a premixture is not physically possible for MFCI. Overall, the main argument of these calculations is that for all premixtures (other than those of unreasonably high melt concentration), the shock wave sweeps in additional coolant such that thermal equilibration of the fragmented melt does not produce the amount of water expansion needed to sustain the wave.

Yuen and Theofanous, [1994] recognized this fundamental problem with the classical thermal detonation theory but also acknowledged experimental evidence of MFCI explosion phenomena that produce strong shock waves. Those authors developed the *microinteractions* model of thermal detonation, which hypothesized that the rate of water mixing with fragmented melt is proportional to the melt fragmentation rate. Chen *et al.* [1995] experimentally verified this model and showed detonation dynamics limited to only what is termed the *m-fluid* (a mixture of fragmented debris and entrained coolant). With those results and successful simulation of MFCI detonation dynamics, Yuen and Theofanous [1999] emphasize that the microinteractions model of thermal detonation is viable; it occurs under much less restrictive premixture conditions and avoids other problems of the classical theory.

For application to the dynamics of water/magma interaction, let us just assume that thermal detonation simply entails shock-wave dynamics that lead to catastrophic fragmentation and expansion of a mixture of magma fragments and water. This generalized view is intended to include the phenomena such as *thermohydraulic fracturing* and *brittle reaction* that Büttner and Zimanowski [1998] and Zimanowski *et al.* [1997b] describe. Zimanowski *et al.* [1997a] describe MFCI experiments that show development of intense shock waves in less than a millisecond with extreme cooling ($>10^6$ K s⁻¹) and stress rates (>3 GPa m⁻²). These phenomena constitute a brittle reaction that occurs on a very fine scale; the brittle reaction is quite different in concept from the detonation idea presented above. However, one can argue that the thermodynamic and hy-

hydrodynamic conditions of this brittle reaction are also those that pertain to detonation. For this reason, I will further consider the broad, generalized concept of thermal detonation and how it might apply to the deep submarine environment.

Figure 9 schematically illustrates the basic idea of thermal detonation. Consider the vapor-film dynamics discussed above and imagine that the contact between a submarine extrusion and seawater forms a salvage zone of unstable vapor and magma fragments. The process leading to explosion of this mixture involves the propagation of a pressure disturbance in the seawater caused by a dynamic event such as volcanic seismicity, vent collapse, or energetic film collapse. As this wave moves through the mixture of hydroclasts, vapor, and water, if its overpressure is great enough, it can compress the vapor into liquid, causing intimate contact with the magma. This contact induces an abrupt increase in overall heat transfer to the water, leading to a pressure jump behind the wave that can drive the wave as a shock. As the shock moves through the mixture, its steep pressure gradient accelerates the water and hydroclasts proportional to their density. This differential acceleration produces a slip velocity between the water and hydroclasts high enough to tear the hydroclasts into micrometer-sized particles, increasing the surface area for heat transfer by orders of magnitude. The increased heat transport caused by the shock wave and the fine fragmentation and expansion in its wake tend to sustain and even enhance the shock. An idealized shock has a *N-wave* profile, and falling pressure in its wake allows expansion and release of thermodynamic work even at high ambient pressure.

In order for this phenomenon to be considered a detonation, the acceleration of the mixture by the shock wave must produce a relative velocity high enough to satisfy the Chapman-Jouguet (C-J) condition: the relative velocity, u_r , is the speed of the shocked material relative to the shock front, and u_r must equal the sonic velocity of the shocked material [Courant and Friedrichs, 1948; and Zel'dovich and Raizer, 1966]. The C-J condition can be evaluated on a pressure-volume diagram that shows the shock adiabat (termed the *shock Hugoniot* and defined as the locus of points representing pressure-volume states achievable by shocking a material from an initial state) and the release adiabat (called the *detonation curve* or *detonation Hugoniot*). These adiabats are concave upward and the detonation curve exists at higher volume states than the shock Hugoniot. Two points on the shock Hugoniot, one at the initial pressure and the other at the pressure of the shock front (the *von Neumann spike*), define a line called the *Rayleigh line*. A C-J condition only exists if the Rayleigh line intersects the detonation curve at a single point of tangency. The points behind a propagating shock at which the C-J condition exists define a surface known as the *C-J*

plane or the *detonation front* (not to be confused with the shock front).

Board *et al.* [1975] and Fauske [1977] suggested that the C-J condition for a water/melt mixture can be met if a propagating shock wave causes melt fragmentation in a time shorter than that required for water-melt velocity equilibration (zero slip velocity). Those authors describe how melt breakup and velocity equilibration times can be assessed by a Bond number function. The Bond number is $3/8$ the product of the coefficient of drag and the Weber number (a ratio of inertial forces to surface tension forces); it is used in calculations of momentum transfer in general, especially for assessing atomization and motion of bubbles and droplets. The Bond number function as envisioned by Bankoff and Jo [1976] includes the effects of phase densities and volume fractions, initial premixture fragment size, the water/melt slip velocity, and the pressure at the shock front and at the C-J plane. With the microinteractions model of Yuen and Theofanous [1999] this function predicts that thermal detonation can occur in MFCIs.

In application of detonation theory there are mitigating factors in hydrovolcanic systems that one should consider. One major factor is that water/magma interaction systems likely involve spatially varying mixture densities and thermodynamic states. Such variations predict nonuniform C-J conditions that tend to destabilize a detonation wave. A second factor is geometry. It is likely that the mixture zone is discontinuous, thin in some places, thick in others. This situation leads to 3-D effects that cause large lateral slip velocities along the shock front, and such slip velocities tend to degrade the sonic conditions behind the front necessary for detonation.

Because the microinteractions model of Yuen and Theofanous [1999] addresses many of the mitigating circumstances in MFCI detonation theory and allows successful prediction of experimental explosions, there is some justification for applying general aspects of that theory to assess the effects of ambient pressure on hydrovolcanism. By assuming that a C-J condition is satisfied by interaction dynamics and that the slip velocity between the shocked melt fragments and water is at least as large as the C-J plane relative velocity [Board *et al.*, 1975], then the Bond number function can be calculated. Board *et al.* [1975] use the Rankine-Hugoniot jump condition [Landau and Lifshitz, 1959; and Zel'dovich and Raizer, 1966] of the propagating shock wave to determine its velocity at ~ 300 m s⁻¹. The relative velocity, u_r , of the shocked mixture leaving the front is given by a function of the mixture's pressure, p , and specific volume, $V = V(R)$, at ambient (subscript *i*) and C-J (subscript *cj*) conditions:

$$u_r = \sqrt{(p_{cj} - p_i)(V_i - V_{cj})} \quad (7)$$

For an idealized thermal detonation in which $p_{cj} \approx 100$ MPa, Board *et al.* [1975] calculated u_r at $\sim 100 \text{ m s}^{-1}$. For MFCI volcano analogs, Wohletz [1986] used the approach suggested by Corradini [1981] to estimate a minimum u_r at 60 m s^{-1} . Drumheller [1979] combined the requirements for relative velocity and melt breakup time into what can be called a critical Bond number. By assuming a constant p_{cj} , Wohletz [1986] evaluated the critical Bond number with respect to FCI experimental data [Wohletz and McQueen, 1984] to predict the effects of R and ambient pressure on the development of relative velocities and magma particle sizes. These results are plotted in Figure 10, which shows optimal conditions for thermal detonation at $0.5 < R < 2.0$ for ambient pressures at or below 40 MPa. With increasing ambient pressure, the predicted relative velocities fall, eventually going below 60 m s^{-1} , which Wohletz [1986] considered as the lower limit for sustaining a detonation. With increasing ambient pressure, particle fragmentation is also decreased, meaning less thermal energy is released in the wake of the shock wave. If these results have any bearing on shock-wave dynamics for water/magma interactions in the submarine environment, then they do suggest that a thermal detonation is not likely at water depths greater than about 4000 m.

6. DISCUSSION

Because observational evidence of deep submarine eruptions is sparse, much of the information I have presented is conceptual and highly theoretical with factual basis going only so far as what analog MFCI experiments and thermodynamic constraints permit. Overall I have described some general factors governing submarine hydrovolcanism and specifically addressed issues concerning the possibility of explosive water/magma interaction at high hydrostatic pressure. I have little or no proof of the predictions presented here, which is a major weakness to this contribution. I have relied upon results of analog experiments designed to quantify the controls of water/melt interaction, attempted thermodynamic analysis of the somewhat complex heat exchange between magma and water, and presented a short review of dominant physical processes that govern the character of interaction.

Chief concerns about application of experimental results to deep submarine eruptions are the experimental water/magma ratios used in high-pressure MFCI studies and the method by which high ambient pressure is experimentally produced. Even though the *water-box* experiments approached R values of 10, these are in no way even close to the *apparent* R values in submarine conditions, which are potentially so large that they are practically impossible to quantify. As I pointed out, from the heat flow mechanisms involved, characteristic times and lengths of thermal diffusion, pressure-wave propagation, and film boiling do

limit the amount of water that can really be involved in interaction over short periods of time. It is because of these limitations, that the *water-box* experiments produced both pillow-lava-like debris, presumably from more passive quenching processes, as well as explosive fragmental debris. These results suggest the upper range of R that is practical for consideration is no larger than 10.

The *water-box* experiments did not employ any kind of confinement to simulate the hydrostatic pressure typical of submarine conditions. For this reason, the high-pressure experiments were examined to test if explosive interaction could occur at ambient pressures above critical pressure. The main concern here is if the ambient pressure generated at the instant of water/melt contact but prior to burst is a plausible analog for hydrostatic pressure. From the standpoint of thermodynamics and physical properties of water, I conclude that this concern is negligible. Because initiation of water/melt interaction causes pressures to rise to near-maximum values in $<< 1 \text{ s}$, it is safe to assume that most of the dynamic heat exchange occurred at the burst pressure. One might argue that in the deep submarine environment this pressure exists before any heat exchange occurs, in contrast to the experiments where the pressure rose in milliseconds prior to interaction. However, the thermodynamic models show that for the initial equilibrium conditions, ambient pressure plays only a small role.

The thermodynamic models presented are limited in applicability because they assume pure water. Whereas this assumption is justifiable for subcritical thermodynamic calculations, because seawater's heat capacity is within a few percent of that of pure water, such may not be the case for supercritical seawater. The effects of phase separation and the extension of the two-phase boundary to supercritical pressures and temperatures place additional energy constraints on isentropic expansion from high temperatures and pressures; further work is needed address the magnitude of these effects for MFCIs. The model discussed in this paper was designed to be applicable to experimental results; its validity is how well it predicts experimental results. For FCI experiments that constrained conversion ratios by kinetic energy measurements, the thermodynamic model proved to be reliable. Unlike controlled experiments, it is not really known how much of water and melt are involved at any given time during submarine hydrovolcanism; the thermodynamic model applied to *apparent* R values tends to give minimum estimates of explosive energy.

From my experience with MFCI experiments and theoretical modeling of water/magma interaction I have focused primarily on R as a controlling parameter. Water/magma mass ratio is really difficult to evaluate, but not impossible as shown by Wohletz [2002]. No matter what approach one uses to constraining R , the *effective* R is controlled by a system's characteristic length and time

scales for heat transfer and hydrodynamics. The example discussed earlier emphasizes that the length scales are a function of diffusivities and sound speed with characteristic times about of about a millisecond per meter of characteristic length for pressure waves propagation. Considering thermal diffusion rates, the volume of water heated is within an order of magnitude of the volume of magma cooled. Thus even though the volume of water available is practically infinite for submarine hydrovolcanism, I suggest that *effective R* values are less than ~10 for submarine volcanism.

As a function of *R*, calculated thermodynamic conversion ratios are a measure of thermodynamic work done by water expansion. One cannot assume that all of this work is manifested as melt-fragment kinetic energy. Wohletz *et al.* [1995] measured FCI ejecta kinetic energy and found it to be typically one-third to one-half the thermodynamic work predicted. Much of the work is spent on melt fragmentation and deformation, seismic and acoustic waves, and viscous losses. This consideration suggests that measures of hydrovolcanic ejecta dispersal (a typical approach to studying terrestrial eruptions) do not fully constrain the eruption energetics. On the other hand, energy calculations based upon crater dimensions do account for most energy expenditures because these calculations are empirical [Wohletz and Heiken, 1992]. For the submarine environment, hydrovolcanic energies may be difficult to constrain because measurement of crater excavation and fragment dispersal are limited by seafloor imaging techniques. That is not to say estimates cannot be done. I recommend making volume estimates of fragmental deposits as a measure of how much magma might have been involved in a submarine hydrovolcanic eruption. The seawater volume involved in such an eruption is more interpretive and requires deduction of the mode of interaction and application of logic similar to that presented in Eqs. (2-4). Then evaluation of Eq. (5) provides a measure of the *effective R* for the eruption from which a thermodynamic conversion ratio can be calculated.

In modeling the expansion work caused by the depressurization of heated water, I presented two bounding thermodynamic cases, *isentropic fluid* and *isentropic mixture* for calculating the conversion of thermal to mechanical energy. If expansion only extends to local hydrostatic pressure, then calculated conversion ratios at high hydrostatic pressures (>200 MPa) exceed the experimentally constrained explosive threshold for a rather limited range of *R* values, which suggests that explosive hydrovolcanism may not be common in deep environments and the *fluid* case of calculation is appropriate. This point of view might be supported by the much more common observations of lava than hydroclasts from deep ocean cores. However, if explosive interaction is triggered, the *mixture* expansion case may be more appropriate, since magma fragmentation adds

the potential for continued heat transfer during water expansion leading to higher conversion ratios.

Thermodynamic modeling also includes two endmember expansion states, a conservative one for which expansion ends at hydrostatic pressure and the other allowing full expansion to atmospheric pressure. If there is real potential for shock-wave dynamics, as in the case of the generalized concept of thermal detonation, localized expansion to pressure much lower than ambient might occur because of spatially varying sonic conditions. Recalling that local sound speeds can vary over an order of magnitude in multiphase systems [e.g., Kieffer, 1977], the rapidly expanding mixture will not “know” when it has reached hydrostatic pressure until a finite time after it has expanded beyond that point to much lower pressures. This aspect is a fundamental of supersonic flow and shock waves, which brings up another aspect of ambient pressure above the critical pressure. Whereas arguments can be made that explosion will not occur at these pressures because the expansion is supercritical and does not involve a large volume change, I emphasize that the dynamics are mostly controlled by how fast the expansion occurs whether or not a distinct vapor phase is present. I also note that most chemical explosives operate far above their critical pressures [e.g., Fordham, 1966], and this has been a criterion that FCI studies [e.g., Yuen and Theofanous, 1999] have used to differentiate detonation phenomena. Based on these considerations, if explosive interaction involves *isentropic mixture* expansion, then the calculations shown in Figure 6 indicate that mechanical energy release increases with ambient pressure, and the details of how high interaction pressure and heat transfer might occur come into question.

In discussion of the affects of ambient pressure on propagation of a hypothetical thermal detonation within a water/melt mixture, I presented some theory and calculations supported by experimental evidence. These calculations showed that with increasing ambient pressure, the range of *R* over which relative velocities support detonation narrows and becomes nonexistent at ambient pressures above 40 MPa. Considering the C-J conditions for a thermal detonation, isothermally or adiabatically increasing ambient pressure decreases water’s specific volume and, assuming a constant detonation curve, increases the slope of the Rayleigh line. If in this case the Rayleigh line were to intersect the detonation curve at two points, a situation of overdriven detonation would occur, which would not be stable. On the other hand, if the Rayleigh line were still tangent to the detonation curve, then its point of tangency would stipulate a higher C-J pressure. A higher C-J pressure causes a higher pressure to exist in the water/melt mixture. If the sound speed of the mixture behaves like the liquid-gas mixtures studied by Kieffer [1977] and increases with pressure, then the relative velocity of the C-J plane should also increase. This consideration (not recognized by

Wohletz [1986]) suggests that curves shown in Figure 10 might plot at higher values of relative velocity for ambient pressures above atmospheric; hence, ambient pressure may not necessarily suppress MFCI detonation.

At this point in time the work of Zimanowski *et al.* [1997a] is perhaps the most plausible description of a mechanism for extremely high energy transfer rates in MFCIs. The tremendously dynamic, brittle reaction discovered by these workers has been photographically documented [Zimanowski *et al.*, 1997b], and it provides a new way for understanding high interaction pressures and heat transfer rates. The hydrodynamics of the brittle reaction have not been linked to detonation, and to do so requires documentation of propagation speeds, sound speeds, and the shock Hugoniot of a water/melt mixture. If a link to detonation were to be established, then a robust predictive capability could be established by scaling experimental work. One such prediction, mentioned earlier, is the hypothetical effect of ambient pressure on the potential for detonation. Even though increasing pressure (depth) might increase the mechanical energy released in a detonation wave, the slip velocity (between the water and melt in a shocked mixture) and the degree of melt fragmentation behind the shock may decrease with increasing pressure, leading to conditions not capable of sustaining a detonation wave. This line of reasoning seems to fit results of high-pressure MFCI experiments discussed above in which the highest energy bursts occurred at the highest confining pressures but the likelihood of non-burst was also higher.

Some aspects of how magma is erupted on the seafloor have not been fully considered. Passive extrusion of flows and domes are suspected to be capable of entrapping water beneath them (producing low *effective R* values) and forming surface selvages of unstable, supercritical fluids and hydroclasts, situations that potentially can be explosive. However, the situation of magma fountaining with magmatic volatile exsolution is another situation seemingly prone to explosive interaction. The fountaining prefragments the magma, resulting in a much greater surface area for heat transfer, and fountaining drives mixing of water with hydroclasts; both processes are important for explosive interaction. If, however, exsolved volatiles are rich in noncondensable gases, such as CO₂, explosive interaction might be damped. Noncondensable gases tend to limit intimate contact of water with the magma by forming a stable insulating film at the magma surface.

7. CONCLUSIONS

By definition, submarine volcanism is hydrovolcanism, but for deep submarine environments it is apparently non-explosive hydrovolcanism, with products of explosive events rarely observed in deep seafloor samples. Do these observations indicate that high hydrostatic pressure pre-

vents explosive interaction, or do they more simply point to the fact that deep seafloor observations are too sparse relative to the vast expanses of the oceans to adequately assess the frequency of explosive products? At this point I conclude that this issue is unresolved.

I do conclude that experimental evidence and theoretical considerations indicate that explosive hydrovolcanism is certainly possible for depths extending to greater than 4000 m. Furthermore theory does point to the potential that if explosions do occur at great depth, then they may release more mechanical energy per unit mass of magma than they would at or near the sea surface. What remains to be studied is how a violent explosion might affect the deep submarine environment (e.g., hydroclast characteristics and dispersal, deposit morphology, vent shape, and seawater currents), taking into consideration the much greater viscous and thermal dissipations existing in the aqueous environment compared to those in subaerial settings.

I also conclude that high ambient pressure may have the potential of decreasing the probability of thermal detonation as a mechanism explosive interaction. But I do emphasize that this conclusion is largely conceptual. The detonation curve for MFCI is yet to be well established, and higher GJ pressures might result for systems at higher ambient pressure. As a final note about thermal detonation, I suggest that MFCI explosions may be better represented by detonations other than the Chapman-Jouguet type [e.g., Rabie *et al.*, 1979; and Wood and Kirkwood, 1954].

At the time of writing this paper, over 30 years have past since focused research on water/magma interaction (hydrovolcanism) began, then if an effort to understand the origins of maar craters and how they might be differentiated from those formed by impact. The early studies [e.g., Fisher, 1968; Lorenz, 1970; Waters and Fisher, 1971; and Heiken, 1971] were perceptive and led to quantitative field techniques, theoretical considerations, and experimental studies [e.g., Sheridan and Wohletz, 1981; Zimanowski *et al.*, 1986; and Kokelaar, 1986]. The identification of phenomenological commonality with industrial vapor explosions, especially those of concern to nuclear reactor safety [e.g., Marshall, 1986], has greatly enhanced the appreciation of the physical controls of hydrovolcanism. However, I conclude that research has a long way to go in developing a fuller understanding of hydrovolcanism, not only of its physical controls but also of its geochemical significance, especially in the submarine environment.

Acknowledgements. This work was done under the auspices of the U.S. Department of Energy. The author thanks James White for enlightening information about submarine volcanism, stimulating discussion of various points of view, and editorial help in adapting this work to suit this volume. Larry Mastin and Magnús Gudmundsson provided detailed and insightful reviews that highlighted the strengths and weaknesses of this work, leading to its

improvement. I am indebted to Bernd Zimanowski and Ralf Büttner for sharing their unique insights into experimental results. Although our conclusions may differ, our common grounds of experience will no doubt stimulate future advances on understanding molten fuel-coolant interactions.

APPENDIX A. CALCULATION OF INTERACTION THERMODYNAMIC WORK

The ratio of thermodynamic work to the magma's heat energy (in excess of ambient) is termed the *conversion ratio*, which is a measure of how dynamic a water/magma interaction is. Passive interactions result in little pressure-volume work so that the conversion ratio is a few percent or less while explosive interactions may show conversion ratios reaching 20% or more. Explosive interactions that tend to keep the expanding water and magma fragments in constant contact and thermal equilibrium show higher conversion ratios than do those where the water separates from the magma during expansion.

Calculation of thermodynamic conversion ratios as a function of R (water/magma mass ratio) provides a theoretical basis for predicting the effects of hydrostatic pressure. These calculations begin with the following assumptions: (1) water is initially saturated (no vapor present); (2) all heat transferred from the magma during interaction is to the water (adiabatic boundary); (3) liquid water is incompressible; and (4) heat exchange is sufficiently rapid that water and magma reach an equilibrium temperature, T_e , before the water expands:

$$T_e = \frac{RC_v T_w + C_m T_m}{RC_v + C_m} , \quad (\text{A-1})$$

where T is temperature (subscripts e for equilibrium, w for water, and m for magma), and C is specific heat, assumed to be constant (subscripts v for water at constant volume and m for magma). Because most of the water stays saturated during attainment of initial thermal equilibrium with magma, its specific heat is nearly constant between T_w and T_e and Eq. (A-1) also assumes this constancy.

The *Hicks-Menzies* [1965] assumption of rapid heat exchange includes the idea that water does not experience much volume change in reaching equilibrium with the melt so that volume terms can be ignored in the derivative of entropy:

$$dS = \frac{C_v}{T} dT + \left(\frac{\partial p}{\partial T} \right)_v dV , \quad (\text{A-2})$$

for which S is entropy, C_v is the constant volume heat capacity, T is temperature, p is pressure and V is volume. Solving Eq. (A-2) for constant volume yields:

$$S_e = S_i + C_v \ln(T_e / T_i) , \quad (\text{A-3})$$

where the subscripts i and e denote the initial (T ambient) and equilibrium states, respectively.

T_e and S_e alone are not sufficient to predict other thermodynamic properties without further considerations. The rapid heating to initial equilibrium temperature and pressure can be idealized as *isochoric* (constant volume), but that idealization is only approached for shock compression of water at low pressure, and it does not allow for the creation of a vapor film at water/melt interfaces, which is documented in MFCI experiments. Accordingly, for the calculated T_e and S_e values, equilibrium states of pressure, volume, and other thermodynamic parameters are determined by fitting polynomial functions to steam-table data [e.g., *Haar et al.*, 1984]. Figure 5a shows water's initial equilibrium specific volume increasing with decreasing R ; however, water's total volume fraction in the mixture decreases with decreasing R such that the effect on the mixture volume is always less than 10%.

With the equilibrium state defined as a function of R , calculation of the final expanded thermodynamic state depends upon whether an *isentropic fluid* or *isentropic mixture* expansion path is followed during water expansion and the final pressure. For calculations, the *fluid* case just requires finding thermodynamic parameters for the desired final pressure at the equilibrium entropy (isentropic expansion). The *mixture* case is a bit more complex [Wohletz, 1986], requiring calculation of the slope of the expansion curve in temperature-entropy space and finding thermodynamic parameters for points (if any) where this curve intersects the saturation curve. The total work for the *mixture* calculation then becomes the sum of the work for each leg of the expansion path.

The First Law of Thermodynamics provides a starting point for calculation of thermodynamic work:

$$dU = dQ + dW , \quad (\text{A-4})$$

for which U is the energy of the system, Q is heat, W is thermodynamic work, p is pressure, and V is volume such that $dW = -pdV$. For a system at constant pressure, $U = H - pV$, $dQ = C_p dT$, and $-W = U_f - U_i$, where H is enthalpy, C_p is the constant pressure heat capacity, and the subscripts f and i denote the final and initial states of the system, respectively. Furthermore at constant pressure, $dU = dQ - pdV$ and $C_p = dU/dT + p(dV/dT) = dQ/dT$. Alternatively, for a system at constant volume, $dU = dQ$, and $C_v = dU/dT = dQ/dT$.

Using the above thermodynamic relationships and the definition of an isentropic adiabatic process as one where $dQ = 0$, $dW = dU$, the mechanical work involved is $dW = (U_i - U_f)$ so that

$$W = (H - pV)_i - (H - pV)_f \quad (A-5)$$

For an *isentropic mixture* process involving magma and water (where m and w are their respective masses), thermodynamic work is the sum of heat transfer and internal energy change, $-dW = dQ - dU$, where heat transfer is $dQ = (mC_m + wC_v)dT + pdV$:

$$-dW = [(mC_m + wC_v)dT + pdV] - dU \quad (A-6)$$

integrating:

$$\begin{aligned} -W &= [(mC_m + wC_v)(T_f - T_i)] \\ &+ [H_f + X_f H_f^* - p(V_f + X_f V_f^*)] \\ &- [H_i + X_i H_i^* - p(V_i + X_i V_i^*)] \\ &- [(H_f - pV_f) - (H_i - pV_i)] \quad (A-7) \end{aligned}$$

and combining terms:

$$\begin{aligned} W &= [(mC_m + wC_v)(T_f - T_i)] \\ &+ [X_i(H_i^* - pV_i^*) - X_f(H_f^* - pV_f^*)] \quad (A-8) \end{aligned}$$

Expansion within the steam dome involves specification of pressure-dependent phase-change enthalpy, H^* , and volume V^* , and calculation of steam fractions, X , by the ratio of entropy S over the phase-change entropy. Whereas calculation of the *isentropic fluid* case by adiabatic expansion is relatively simple, application of Eq. (A-8) requires careful consideration of thermodynamic path. If expansion does not go through the steam dome, phase-change terms do not apply so that one should use:

$$\begin{aligned} W &= [(mC_m + wC_v)(T_f - T_i)] \\ &- [(H_f - pV_f) - (H_i - pV_i)] \quad (A-9) \end{aligned}$$

Numerical implementation of this calculation involves steam-table lookups for which the author has written a computer program with built-in thermodynamic property calculations that are accurate within 1% of values listed in steam tables [Lemmon *et al.*, 2001]. This program may be downloaded from the internet by contacting the author.

REFERENCES

Angelini, S., Takara, E., Yuen, W. W., and T. G. Theofanous, Multiphase transients in the premixing of steam explosions, *Nucl. Eng. Des.*, 146, 83-95, 1994.

- Angelini, S., Theofanous, T. G. and W. W. Yuen, The mixing of particle clouds plunging into water, *Nucl. Eng. Des.*, 177, 285-301, 1994.
- Bankoff, S. G., and J. H. Jo, Existence of steady-state fuel-coolant thermal detonation waves, ERDA Rep. NU-2512-6 (CONF-760328-8), National Technical Information Service, Springfield, VA, 1976.
- Batiza, R., D. J. Fornari, D. A. Vanko, and P. Lonsdale, Craters, calderas, and hyaloclastites on young Pacific seamounts, *J. Geophys. Res.*, 89, 8371-8390, 1984.
- Bischoff, J. L., and R. J. Rosenbauer, The critical point and two-phase boundary of seawater, 200-500°C, *Earth Planet. Sci. Lett.*, 68, 172-180, 1984.
- Bischoff, J. L., and R. J. Rosenbauer, Liquid-vapor relations in the critical region of the system NaCl-H₂O from 380 to 415°C: a refined determination of the critical point and two-phase boundary of seawater, *Geochim. Cosmochim. Acta*, 52, 2121-2126, 1988.
- Board, S. J., R. W. Hall, and R. S. Hall, Detonation of fuel coolant explosions, *Nature*, 254, 319-321, 1975.
- Bonatti, E., Mechanisms of deep sea volcanism in the South Pacific, in *Researches in Geochemistry*, 2, edited by P. H. Ableson, pp. 453-491, John Wiley & Sons, New York, 1967.
- Buntebarth, G., and J. R. Schopper, Experimental and theoretical investigations on the influence of fluids, solids and interactions between them on thermal properties of porous rocks, *Phys. Chem. Earth*, (23)9-10: 1141-1146, 1998.
- Burnham, C. W., Energy of explosive volcanic eruptions, *Sci.*, 213, 69-70, 1981.
- Burnham, C., Deep submarine pyroclastic eruptions, *Econ. Geol., Monograph* 5, 142-148, 1983.
- Büttner, R., and B. Zimanowski, Physics of thermohydraulic explosions, *Phys. Review E*, 57-5, 1-4, 1998.
- Buxton, L. D.; and W. B. Benedict, Steam explosion efficiency studies, Sandia National Laboratories Report, SAND79-1399, NUREG/CR-0947, 62 pp., NTIS, Springfield, Virginia, 1979.
- Chen, X., Yuen, W. W., and T. G. Theofanous, On the constitutive description of the microinteractions concept in steam explosions, *Nucl. Eng. Des.*, 177, 303-319.
- Clague, D. A., Davis, A. S., Bischoff, J. L., Dixon, H. E., and R. Geyer, Lava bubble-wall fragments formed by submarine hydrovolcanic explosions on Loihi Seamount and Kilauea Volcano, *Bull. Volcanol.*, 61, 437-449, 2000.
- Clague, D. A., Davis, A. S., and H. E. Dixon, Submarine Strombolian eruptions on the Gorda mid-ocean ridge, (this volume).
- Colgate, S. A., and T. Sigurgeirsson, Dynamic mixing of water and lava, *Nature*, 244, 552-555., 1973..
- Condiff, D., Contributions concerning quasi-steady propagation of thermal detonations, *Int. J. Heat Mass Transfer*, 25, 87-98, 1982.
- Corradini, M. L., Analysis and modeling of steam explosion experiments, Sandia National Laboratories SAND80-2131, NUREG/CR-2072, 114 pp, NTIS, Springfield, Virginia, 1981.
- Cotton, C. A., The pedestals of oceanic volcanic islands, *Geol. Soc. Amer. Bull.*, 80, 749-760, 1969.
- Courant, R., and K. O. Friedrichs, *Supersonic Flow and Shock Waves*, 464 pp., Springer, New York, 1948.
- Dinh, T.N., Dinh, A. T., Nourgaliev, R. R., and B. R. Sehgal, Investigation of film boiling thermal hydraulics under FCI

- conditions, in *Proc. of OECD/CSNI Specialists Meeting on Fuel Coolant Interactions*, Tokai, Japan, May 19-21, 1997, pp. 674-695, Nuclear Energy Agency (France) CSNI R(97)26, 1998.
- Dudás, F. O., The effect of volatile content on the vesiculation of submarine basalt. *Econ. Geol. Mono.* 5, 134-141, 1983.
- Drumheller, D. S., The initiation of melt fragmentation in fuel-coolant interactions, *Nucl. Sci. Eng.*, 72, 347-356, 1979.
- Fauske, H. K., Some comments on shock-induced fragmentation and detonating thermal explosions, *Am. Nucl. Soc. Trans.*, 27, 666-667, 1977.
- Fisher, R. V., Puu Hou littoral cones, Hawaii, *Geol. Rundschau*, 57, 837-864, 1968.
- Fletcher, D. F., and T. G. Theofanous, Heat transfer and fluid dynamic aspects of explosive melt-water interactions, *Adv. Heat Trans.: Heat Trans. Nucl. React. Safety*, 29, 129-213, 1997.
- Fletcher, D. F., and A. Thyagaraja, The CHYMES coarse mixing model, *Prog. Nucl. Ener.*, 26, 31-61, 1991.
- Fordham, S., *High Explosives and Propellants*, Pergamon, New York, 1966.
- Fowles, G. R., Vapor phase explosions: elementary detonations? *Sci.*, 204, 168-169, 1979.
- Haar, L., Gallagher, J. S., and G. S. Kell, *NBS/NRC Steam Tables*, McGraw-Hill International Book Company, London, 320 pp, 1984.
- Harlow, F. H., and H. M. Ruppel, Propagation of a liquid-liquid explosion, Los Alamos National Laboratory Report, LA-8971-MS, 11 pp., NTIS, Springfield, Virginia, 1981.
- Haymon, R. M., Fornari D. J., Von Damm, K. L., Lilley, M. D., Perfit, M. R., Edmond, J. M., Shanks, III, W. C., Lutz, R. A., Grebmeier, J. M., Carbotte, S., Wright, D., McLaughlin, E., Smith, M., Beedle, N., and E. Olsen, Volcanic eruption of the mid-ocean ridge along the East Pacific Rise crest at 9°45'-52'N: Direct submersible observations of seafloor phenomena associated with an eruption event in April, 1991, *Earth Planet. Sci. Let.*, 119, 85-101, 1993.
- Head, J.W. III, and L. Wilson, Deep submarine pyroclastic eruptions: theory and predicted landforms and deposits, (this volume).
- Heiken, G., Tuff rings: examples from the Fort Rock-Christmas Lake Valley, south-central Oregon, *J. Geophys. Res.*, 76, 5615-5626, 1971.
- Hicks, E. P., and D. C. Menzies, Theoretical studies on the fast reactor maximum accident, in *Proceedings of the Conference on Safety, Fuels, and Core Design in Large Fast Power Reactors*, USAEC Rep. ANL-7120, pp. 654-670, Nat. Tech. Inform. Serv., Springfield, Virginia, 1965.
- Honnorez, H., and P. Kirst, Submarine basaltic volcanism: morphometric parameters for discriminating hyaloclastites from hyalotuffs, *Bull. Volcanol.*, 39, 441-465, 1975.
- Kieffer, S. W., Sound speeds in liquid-gas mixtures: water-air and water-steam, *J. Geophys. Res.*, 82, 2895-2904, 1977.
- Kieffer, S. W., and J. M. Delany, Isentropic decompression of fluids from crustal and mantle pressures, *J. Geophys. Res.*, 84, 1611-1620, 1979.
- Kokelaar, P., Magma-water interactions in subaqueous and emergent basaltic volcanism, *Bull. Volcanol.* 48, 275-290, 1986.
- Krauskopf, K. B., *Introduction to Geochemistry*, McGraw-Hill, New York, 721 pp., 1967.
- Landau, L. D., and B. M. Lifshitz, *Fluid Mechanics: Vol 6, Course of Theoretical Physics*, Pergamon, New York, 1959.
- Lemmon, W., M.O. McLinden, and D.G. Friend, Thermophysical properties of fluid systems: in *NIST Chemistry WebBook, NIST Standard Reference Database Number 69*, edited by P. J. Linstrom and W.G. Mallard, National Institute of Standards and Technology, Gaithersburg MD, 2001.
- Lonsdale, P., and R. Batiza, Submersible study of hyaloclastite and lava flows on young seamounts at the mantle of the Gulf of California, *Bull. Geol. Soc. Amer.*, 91, 545-554, 1980.
- Lorenz, V., Some aspects of the eruption mechanism of the Big Hole Maar, central Oregon, *Geol. Soc. Amer. Bull.*, 81, 1823-1830, 1970.
- Maicher, D., White, J. D. L., and R. Batiza, Sheet hyaloclastite: density-current deposits of quench and bubble-burst fragments from thin, glassy sheet lava flows, Seamount Six, Eastern Pacific Ocean, *Marine Geol.*, 171, 75-94, 2000.
- Maicher D., and J. D. L. White, The formation of deep-sea limu o' Pelee, *Bull. Volcanol.*, 63, 482-496, 2001.
- Marshall, E., The lessons of Chernobyl, *Sci.*, 233, 1375-1376, 1986.
- Mattox, T. N., and M. T. Mangan, Littoral hydrovolcanic explosions: a case study of lava-seawater interaction at Kilauea Volcano, *J. Volcanol. Geotherm. Res.*, 75, 1-17, 1997.
- McBirney, A. R., Factors governing the nature of submarine volcanism, *Bull. Volcanol.*, 26, 455-469, 1963.
- Ort M.H., Wohletz, K., Hooten, J. A., Neal, C. A., and V. S. McConnel, The Ukinrek maars eruption, Alaska, 1977: a natural laboratory for the study of phreatomagmatic processes at maars, *Terra Nostra*, 2000/6, 396-400, 2000.
- Peckover, R.S., Buchanan, D. J., and D. E. Ashby, Fuel-coolant interactions in submarine volcanism, *Nature*, 245, 308-308, 1973.
- Rabie, R. L., Fowles, G. R., and W. Fickett, The polymorphic detonation, *Phys. Fluids*, 22, 422-435, 1979.
- Ruggles, A E., Drew, D. A., Lahey, R. T., Jr., and H. A. Scarton, The relationship between standing waves, pressure pulse propagation and the critical flow rate in two-phase mixtures, *J. Heat Trans.*, 111(2), 467-473, 1989.
- Ruggles, A. E., Vasiliev, A. D., Brown, N. W., and M. W. Wendel, role of heater thermal response in reactor thermal limits during oscillatory two-phase flows, *Nucl. Sci. Engin.*, 125, 75-83, 1997.
- Self, S., Wilson, L., and I. A. Nairn, Vulcanian eruption mechanisms, *Nature*, 277, 440-443, 1979.
- Sharon, A., and S. G. Bankoff, On the existence of steady supercritical plane thermal detonations, *Int. J. Mass Heat Trans.*, 24, 1561-1572, 1981.
- Sheridan, M. F.; and K. H. Wohletz, Hydrovolcanic eruptions I. The systematics of water-pyroclast equilibration. *Sci.*, 212, 1387-1389, 1981.
- Sheridan, M. F., and K. H. Wohletz, Hydrovolcanism: basic considerations and review, *J. Volcanol. Geotherm. Res.*, 17, 1-29, 1983.

- Smith, T. L., and R. Batiza, New field and laboratory evidence for the origin of hyaloclastite flows on seamount summits, *Bull. Volcanol.*, 51, 96-114, 1989.
- Sourirajan, S., and G. C. Kennedy, The system H_2O -NaCl at elevated temperatures and pressures, *Am. J. Sci.*, 260, 115-141, 1962.
- Stoffers, P., Worthington, T., Hekinian, R., Petersen, S., Hannington, M., Rurkay, M., and the SO 157 Shipboard Scientific Party, Silicic volcanism and hydrothermal activity documented at Pacific-Antarctic ridge, *EOS Trans. Amer. Geophys. Un.*, 83(28), 301-304, 2002.
- Tanimura, S., Date, J., Takahashi, T., and H. Ohmoto, Geologic setting of the Kuroko deposits in the Hokuroku district: Part II. Stratigraphy and structure of the Hokoroku district, *Econ. Geol. Mono.*, 5, 24-38, 1983.
- Turekian, K. K., *Oceans*, Prentice-Hall, New Jersey, 150 pp, 1968.
- Waters, A. C., and R. V. Fisher, Base surges and their deposits: Capelinhos and Taal volcanoes, *J. Geophys. Res.*, 76, 5596-5614, 1971.
- Wentworth, C. K., Ash formations of the island of Hawaii. Hawaii Volcano Observatory, 3rd Spec. Rep., 173 pp., Hawaiian Volcano Research Society, Honolulu, 1938.
- White, J. D. L., Impure coolants and interaction dynamics of phreatomagmatic eruptions, *Jour. Volcanol. Geotherm. Res.*, 74, 155-170, 1996.
- Wohletz, K. H., Mechanisms of hydrovolcanic pyroclast formation: grain-size, scanning electron microscopy, and experimental results, *Jour. Volcanol. Geotherm. Res.*, 17, 31-63, 1983.
- Wohletz, K. H., Explosive magma-water interactions: Thermodynamics, explosion mechanisms, and field studies, *Bull. Volcanol.*, 48, 245-264, 1986.
- Wohletz, K. H., Water/magma interaction: some theory and experiments on peperite formation. *J. Volcanol. Geotherm. Res.*, 114, 19-35, 2002.
- Wohletz, K. H., and G. Heiken, *Volcanology and geothermal energy*, University of California Press, Berkeley, California, 1992.
- Wohletz, K., and R. G. McQueen, Experimental studies of hydromagmatic volcanism. in *Explosive Volcanism: Inception, Evolution, and Hazards*, pp. 158-169, Studies in Geophysics, National Academy Press, Washington, 1984.
- Wohletz, K. H., McQueen, R. G., and M. Morrissey, Analysis of fuel-coolant interaction experimental analogs of hydrovolcanism, in *Intense Multiphase Interactions*, edited by T. G. Theofanous, and M. Akiyama, pp. 287-317, Proceedings of US (NSF) Japan (JSPS) Joint Seminar, Santa Barbara, CA, June 8-13, 1995, 1995.
- Wood, W. W.; and J. G. Kirkwood, Diameter effect in condensed explosives, *J. Chem. Phys.*, 22, 1920-1924, 1954.
- Yuen, W. W., and T. G. Theofanous, The prediction of 2D thermal detonations and resulting damage potential, *Nucl. Eng. Design*, 155, 289-309, 1994.
- Yuen, W. W., and T. G. Theofanous, On the existence of multiphase thermal detonations, *Proc. Int. J. Multiphase Flow*, 25, 1505-1519, 1999.
- Zel'dovich, Ya. B., and Yu. P. Raizer, *Physics of Shock Waves and High-Temperature Hydrodynamic Phenomena*, Volume I and II, Academic Press, New York, 1966.
- Zimanowski, B., and R. Büttner, Phreatomagmatic explosions in subaqueous volcanism? (this volume).
- Zimanowski, B., Büttner, R., Lorenz, V., and H.-G. Häfele, Fragmentation of basaltic melt in the course of explosive volcanism, *J. Geophys. Res.*, 107, 803-814, 1997a.
- Zimanowski, B., Büttner, R., and J. Nestler, Brittle reaction of a high-temperature ion melt, *Europhys. Lett.*, 38(4), 285-289, 1997b.
- Zimanowski, B., Lorenz, V., and G. Fröhlich, Experiments on phreatomagmatic explosions with silicate and carbonatitic melts, *J. Volcanol. Geotherm. Res.*, 30, 149-153, 1986.
- Zimanowski, B., Fröhlich, G., and V. Lorenz, Quantitative experiments on phreatomagmatic explosions, *J. Volcanol. Geotherm. Res.*, 48, 341-358, 1991.

Kenneth H. Wohletz, Earth and Environmental Sciences, Los Alamos National Laboratory, Los Alamos, New Mexico 87545 USA

FIGURE AND PLATE CAPTIONS (single column)

Figure 1. Schematic illustration of four hypothetical modes of deep submarine extrusion.

Figure 2. (a) Pressure-temperature diagram for the system NaCl-H₂O adapted from Krauskopf [1967] from experimental data from Sourirajan and Kennedy [1962]. This diagram is an overlay for the pure H₂O and NaCl endmembers (dashed lines). The solid lines (bold are experimental data) schematically represent the phase boundaries connecting the pure endmembers. T_w and C_w denote the triple point and critical points of H₂O respectively; T_s and C_s those points for NaCl. (b) The two-phase curve for standard seawater (3.2% NaCl) as a function of pressure and temperature, based on data from Bischoff and Rosenbauer [1984]. Note that in this plot, pressure increases downward. The solid curve designates the boundary where pure water and seawater boundary are nearly coincidental. The boundary for pure water terminates at its critical point, whereas the boundary for seawater extends (dashed curve) to its respective critical point, along which it separates the stability regions of liquid and a mixture of low-salinity vapor and liquid. The phase boundary extends (dotted curve) from seawater's critical point to higher temperature and pressures, separating the liquid region from that of a mixture of high-salinity vapor and brine.

Figure 3. Variation of physical properties of water at 30 MPa (~3000 m depth) and 60 MPa (~6000 m depth) as a function of temperature. The symbols and units for the curves are: **a**—isobaric expansion coefficient (10^3 K^{-1}); **a/b**—pressure coefficient [$(dp/dt)_v$; $10^{-2} \text{ MPa K}^{-1}$] where **b** is the isothermal expansion coefficient; **n**—kinematic viscosity ($10^{-7} \text{ m}^2 \text{ s}^{-1}$); and C_p —the constant pressure heat capacity ($4.184 \times \text{kJ kg}^{-1} \text{ K}^{-1}$). Note the sharp inflections and discontinuities apparent near the critical temperature.

Figure 4. Example pressure records from MFCI experiments designed to study interaction at high confining pressure. Dashed and dotted curves are records from multiple pressure transducers. The designed bursting pressure for these examples are (a) 16.3 MPa, (b) 6.8 MPa, (c) 16.3 MPa, (d) 35.7 MPa, (e) 35.7 MPa, and (f) 16.3 MPa. For the example shown in d, the pressure records do not show the experiment reached designed burst pressure even though burst did occur as shown by the rapid pressure fall off; this behavior was later found to be caused by failure of the burst diaphragm thermal insulation.

Figure 5. Thermodynamic phase diagrams (L is liquid, V is vapor) for calculated water/magma interactions at different water/magma mass ratios, R . Initial equilibrium states are diamond-shaped points; filled circles represent expanded states; and CP is the critical point. (a) A pressure-volume phase diagram illustrates *isentropic fluid* expansion with example expansion isentropes labeled. Note that all 0.1-MPa expanded states are within the steam dome, but those at 10.0 MPa are not. (b) A temperature-entropy phase diagram shows calculated effects of ambient pressure on the initial equilibrium state as a function of R . The solid line with diamond-shaped points is are equilibrium states at 0.1-

MPa ambient pressure, dashed lines are equilibrium states with increasing ambient pressures (10, 20, 40, 60, and 80 MPa) plotting increasingly to the left. This plot also shows *isentropic mixture* expansion final states (0.1 and 10.0 MPa) with schematically drawn lines connecting initial and final states for example R values.

Figure 6. Thermodynamic conversion ratios for *isentropic fluid* plotted as a function of R (water/magma mass ratio). Curves are numbered according to ambient hydrostatic pressure (MPa), and the division between in explosive and effusive is arbitrarily fit to observations of terrestrial (0.1 MPa) eruptions. The four plots illustrate two expansion cases (*isentropic fluid* and *isentropic mixture*) each with two endmember expansion endmembers (hydrostatic and 0.1 MPa).

Figure 7. Schematic illustration of determination of characteristic length scales that determine effective water/magma mass ratios, R .

Figure 8. Schematic illustration of vapor film expansion and collapse, diagrammatically plotting the conductive factor as a function of film thickness and the pressure factor (a ratio of film pressure to ambient), both dimensionless.

Figure 9. Schematic illustration of the concept of thermal detonation [adapted from Wohletz, 1986; and Board et al., 1975], showing the propagation of a shock wave through a coarse mixture of magma fragments and water (vapor and liquid). The shock wave moves at a velocity u and differentially accelerates the water and magma to velocities of u_w and u_m , respectively, resulting in a slip velocity u_s , which decays behind the shock. The slip velocity must be of sufficient amplitude to cause fine fragmentation of the magma fragments by mechanisms such as boundary layer stripping and Taylor instability before the arrival of the C-J plane. At the C-J plane the average mixture velocity is just sonic (c) with respect to the shock wave. The fine fragmentation causes an exponential rise in heat transfer from the magma fragments to the water and catastrophic vapor expansion.

Figure 10. Calculated effect of ambient pressure on thermal detonation relative velocities and fragment size as a function of R (water/magma mass ratio) and ambient pressure [from Wohletz, 1986].

Plate 1. Photograph of the *water box* experiment, consisting of a Plexiglas box about 1 m on a side, filled with water, and enclosing a cylindrical container of thermite, prior to ignition.

Plate 2. Photograph of a *water box* experiment in action. The interaction ejected centimeter-size fragments of molten thermite in ballistic trajectories like a Strombolian eruption. At the same time, not visible in this picture, molten globs of thermite spread like pillow lava over the floor of the box.

Plate 3. Confinement vessel being pressure-tested. The vessel is about 1 m high and 0.4 m in diameter. The central vent tube (~0.1m diameter) visible at the vessel top extends to the base of

the cylinder into a compartment holding water with the thermite place above. The base of the vent tube is sealed with a burst diaphragm welded in place. Burst diaphragms were constructed from aluminum plates and machined with crossing grooves, the depth of which determined the burst strength. These diaphragms (also called *petal valves* because their failure resembled the opening flower petals) were calibrated by the above pressure test, and the maximum confinement design was 35.7 MPa.

Plate 4. A supersonic jet of molten thermite dust and superheated steam vents to heights of >30 m from an experimental vessel about 1 m high (just visible in the far right photograph). These images display the violence of high-pressure interaction of water with melt.

FIGURE AND PLATE CAPTIONS (two column)

Figure 1. Schematic illustration of four hypothetical modes of deep submarine extrusion.

Figure 2. (a) Pressure-temperature diagram for the system NaCl-H₂O adapted from *Krauskopf* [1967] from experimental data from *Sourirajan and Kennedy* [1962]. This diagram is an overlay for the pure H₂O and NaCl endmembers (dashed lines). The solid lines (bold are experimental data) schematically represent the phase boundaries connecting the pure endmembers. T_w and C_w denote the triple point and critical points of H₂O respectively; T_s and C_s those points for NaCl. (b) The two-phase curve for standard seawater (3.2% NaCl) as a function of pressure and temperature, based on data from *Bischoff and Rosenbauer* [1984]. Note that in this plot, pressure increases downward. The solid curve designates the boundary where pure water and seawater boundary are nearly coincidental. The boundary for pure water terminates at its critical point, whereas the boundary for seawater extends (dashed curve) to its respective critical point, along which it separates the stability regions of liquid and a mixture of low-salinity vapor and liquid. The phase boundary extends (dotted curve) from seawater's critical point to higher temperature and pressures, separating the liquid region from that of a mixture of high-salinity vapor and brine.

Figure 3. Variation of physical properties of water at 30 MPa (~3000 m depth) and 60 MPa (~6000 m depth) as a function of temperature. The symbols and units for the curves are: **a**—isobaric expansion coefficient (10^3 K^{-1}); **a/b**—pressure coefficient [$(dp/dt)_v$; $10^{-2} \text{ MPa K}^{-1}$] where **b** is the isothermal expansion coefficient; **n**—kinematic viscosity ($10^{-7} \text{ m}^2 \text{ s}^{-1}$); and C_p —the constant pressure heat capacity ($4.184 \times \text{kJ kg}^{-1} \text{ K}^{-1}$). Note the sharp inflections and discontinuities apparent near the critical temperature.

Figure 4. Example pressure records from MFCI experiments designed to study interaction at high confining pressure. Dashed and dotted curves are records from multiple pressure transducers. The designed bursting pressure for these examples are (a) 16.3 MPa, (b) 6.8 MPa, (c) 16.3 MPa, (d) 35.7 MPa, (e) 35.7 MPa, and (f) 16.3 MPa. For the example shown in d, the pressure records do not show the experiment reached designed burst pressure even though burst did occur as shown by the rapid pressure fall off; this behavior was later found to be caused by failure of the burst diaphragm thermal insulation.

Figure 5. Thermodynamic phase diagrams (*L* is liquid, *V* is vapor) for calculated water/magma interactions at different water/magma mass ratios, *R*. Initial equilibrium states are diamond-shaped points; filled circles represent expanded states; and *CP* is the critical point. (a) A pressure-volume phase diagram illustrates *isentropic fluid* expansion with example expansion isentropes labeled. Note that all 0.1-MPa expanded states are within the steam dome, but those at 10.0 MPa are not. (b) A temperature-entropy phase diagram shows calculated effects of ambient pressure on the initial equilibrium state as a function of *R*. The solid line with diamond-shaped points is are equilibrium states at 0.1-MPa ambient pressure, dashed lines are equilibrium states with increasing ambient pressures (10, 20, 40, 60, and 80 MPa) plotting increasingly to the left. This plot also shows *isentropic mixture* expansion final states (0.1 and 10.0 MPa) with schematically drawn lines connecting initial and final states for example *R* values.

Figure 6. Thermodynamic conversion ratios for *isentropic fluid* plotted as a function of *R* (water/magma mass ratio). Curves are numbered according to ambient hydrostatic pressure (MPa), and the division between explosive and effusive is arbitrarily fit to observations of terrestrial (0.1 MPa) eruptions. The four plots illustrate two expansion cases (*isentropic fluid* and *isentropic mixture*) each with two endmember expansion endmembers (hydrostatic and 0.1 MPa).

Figure 7. Schematic illustration of determination of characteristic length scales that determine effective water/magma mass ratios, *R*.

Figure 8. Schematic illustration of vapor film expansion and collapse, diagrammatically plotting the conductive factor as a function of film thickness and the pressure factor (a ratio of film pressure to ambient), both dimensionless.

Figure 9. Schematic illustration of the concept of thermal detonation [adapted from *Wohletz*, 1986; and *Board et al.*, 1975], showing the propagation of a shock wave through a coarse mixture of magma fragments and water (vapor and liquid). The shock wave moves at a velocity *u* and differentially accelerates the water and magma to velocities of u_w and u_m , respectively, resulting in a slip velocity u_s , which decays behind the shock. The slip velocity must be of sufficient amplitude to cause fine fragmentation of the magma fragments by mechanisms such as boundary layer stripping and Taylor instability before the arrival of the C-J plane. At the C-J plane the average mixture velocity is just sonic (*c*) with respect to the shock wave. The fine fragmentation causes an exponential rise in heat transfer from the magma fragments to the water and catastrophic vapor expansion.

Figure 10. Calculated effect of ambient pressure on thermal detonation relative velocities and fragment size as a function of R (water/magma mass ratio) and ambient pressure [from *Wohletz*, 1986].

Plate 1. Photograph of the *water box* experiment, consisting of a Plexiglas box about 1 m on a side, filled with water, and enclosing a cylindrical container of thermite, prior to ignition.

Plate 2. Photograph of a *water box* experiment in action. The interaction ejected centimeter-size fragments of molten thermite in ballistic trajectories like a Strombolian eruption. At the same time, not visible in this picture, molten globs of thermite spread like pillow lava over the floor of the box.

Plate 3. Confinement vessel being pressure-tested. The vessel is about 1 m high and 0.4 m in diameter. The central vent tube (~0.1m diameter) visible at the vessel top extends to the base of the cylinder into a compartment holding water with the thermite placed above. The base of the vent tube is sealed with a burst diaphragm welded in place. Burst diaphragms were constructed from aluminum plates and machined with crossing grooves, the depth of which determined the burst strength. These diaphragms (also called *petal valves* because their failure resembled the opening flower petals) were calibrated by the above pressure test, and the maximum confinement design was 35.7 MPa.

Plate 4. A supersonic jet of molten thermite dust and superheated steam vents to heights of >30 m from an experimental vessel about 1 m high (just visible in the far right photograph). These images display the violence of high-pressure interaction of water with melt.

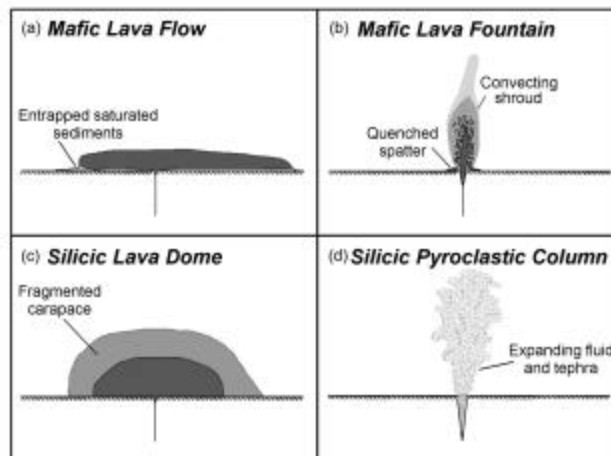


Figure 1.

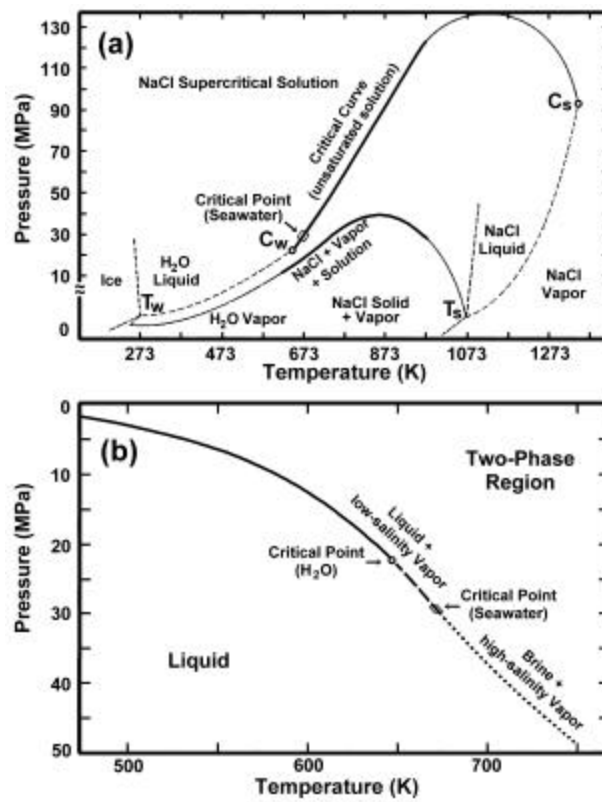


Figure 2.

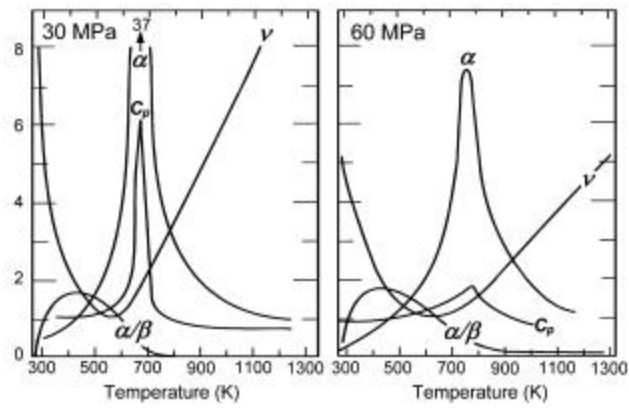


Figure 3.

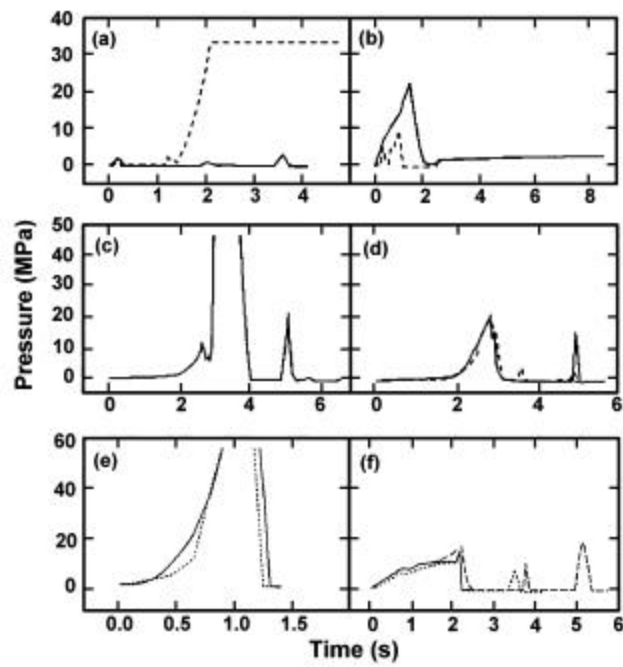


Figure 4.

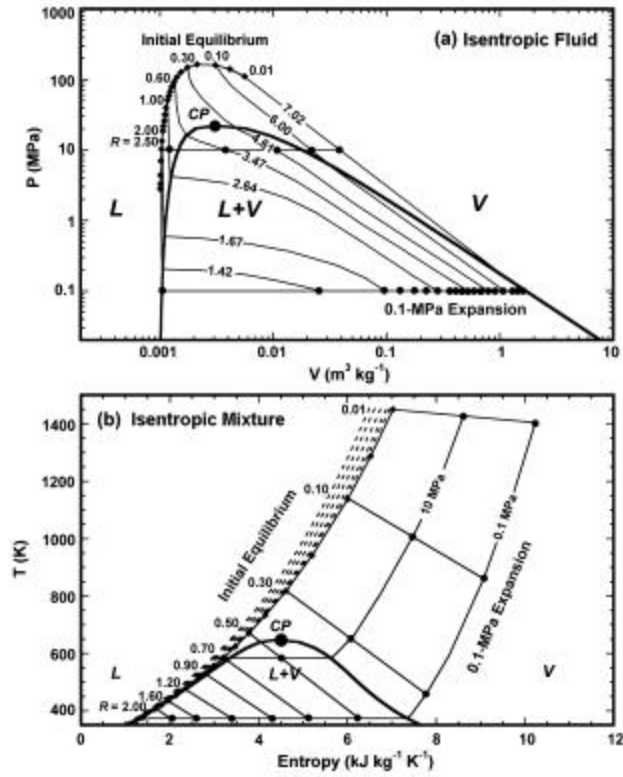


Figure 5.

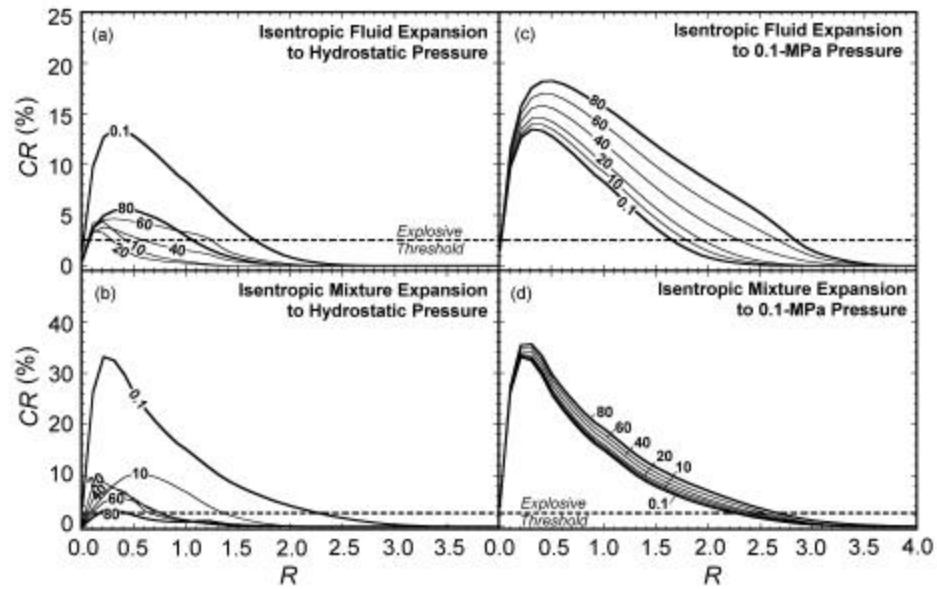


Figure 6.

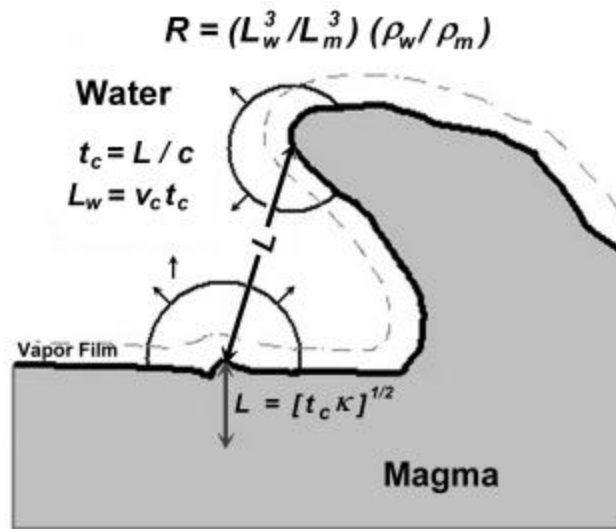


Figure 7.

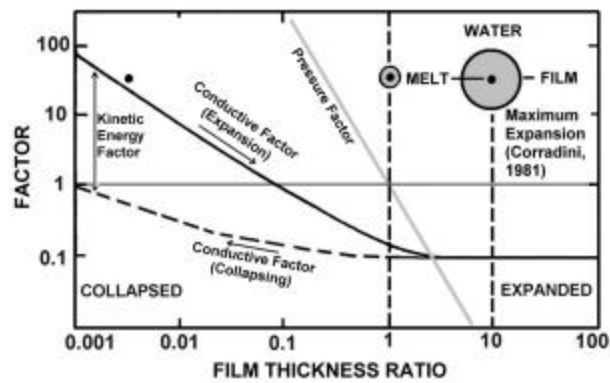


Figure 8.

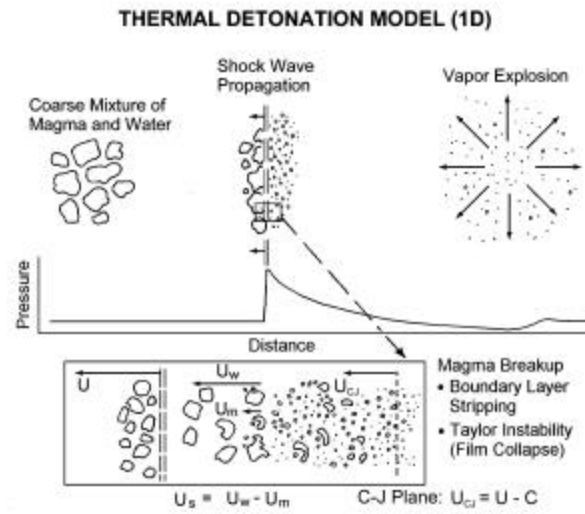


Figure 9.

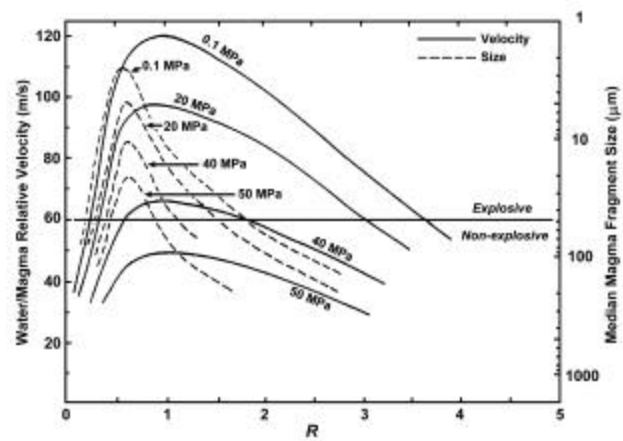


Figure 10.



Plate 1.



Plate 2.



Plate 3.



Plate 4.